Title
Pore-Size-Distribution of Cationic Polyacrylamide Hydrogels (Progress Report)

Authors
Kremer, M.
Prausnitz, John M.

Publication Date
1992-06-01

LBL-32845
UC-401

Lawrence Berkeley Laboratory
UNIVERSITY OF CALIFORNIA

CHEMICAL SCIENCES DIVISION

Pore-Size-Distribution of Cationic Polyacrylamide Hydrogels (Progress Report)

M. Kremer and J.M. Prausnitz

June 1992

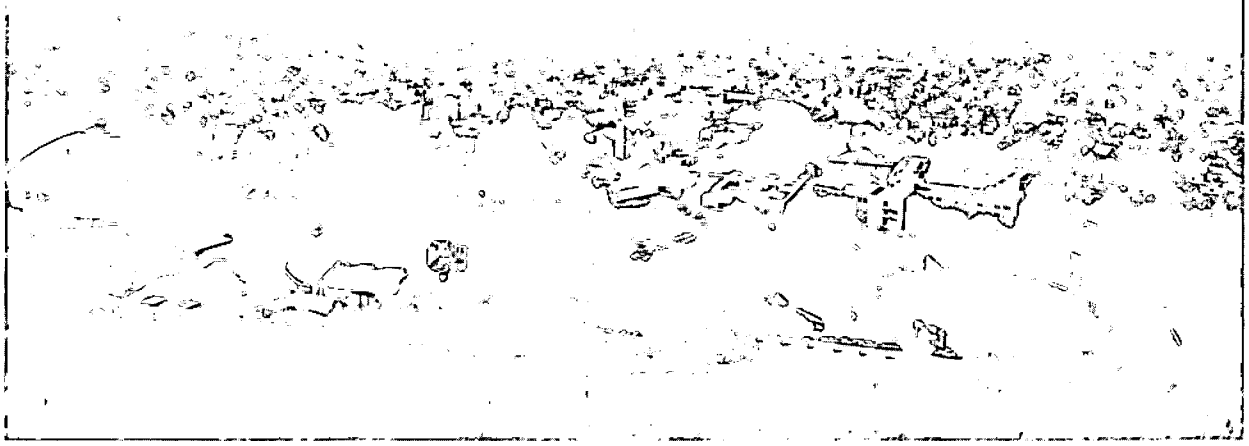

Prepared for the U.S. Department of Energy under Contract Number DE-AC03-76SF00098

DISCLAIMER

DISCLAIMER

LBL-32845

UC-401

Pore-Size-Distribution of Cationic Polyacrylamide Hydrogels

(Progress Report)

Michael Kremer and John M. Prausnitz*

Department of Chemical Engineering

and

Chemical Sciences Division
Lawrence Berkeley Laboratory
University of California, Berkeley
1 Cyclotron Road
Berkeley, CA 94720

June 1992

This work was supported by the Director, Office of Energy Research, Office of Basic Energy Sciences, Chemical Sciences Division of the U.S. Department of Energy under Contract Number DE-AC03-76SF00098

*To whom correspondence should be addressed.

CONTENTS

1. Abstract

Determination of pore-size distributions of porous hydrogels swollen in a liquid medium is a delicate task. Classical methods for investigation of porous structures (mercury intrusion, gas adsorption) are not applicable because the pore structure is supported by the liquid medium and hence not accessible for other liquid or gaseous media.

In this work we used the Mixed-Solute-Exclusion Method, an indirect method to investigate pore structure. For the polyelectrolyte hydrogel, we copolymerized acrylamide (AAm) with the cationic monomer (3-Methacrylamidopropyl) trimethylammonium chloride (MAPTAC) and crosslinked with N,N'-methylenbisacrylamide (BIS). Aqueous solutions with dissolved Dextran- and Poly (ethylene glycol/oxide) molecules of known concentrations, covering a wide range of molecular weight, are brought into contact with the hydrogel. Due to penetration of the various solutes into the gel and the migration of imbibed water out of the gel (caused by difference in osmotic pressure), the coexisting solution phase in equilibrium with the gel has a modified concentration of solutes. Based on this difference of concentrations, the amount of non-accessible water for a solute as a function of molecular weight can be determined. The conversion of the molecular weight of each solute into a solute radius is performed with the aid of hydrodynamic volume theory. With these results, calculation of the pore-size distribution is feasible by solving the Fredholm-equation.

To show the feasibility of this indirect method, we compare known pore-sizes of porous structures with the results of the mixed-SE method (in conjunction with the solution of the Fredholm-equation). Theoretical studies are accompanied by an experimental investigation of the pore stucture of an AAm/MAPTAC hydrogel.

Our results confirm the feasibility of determining pore-size distribution of porous materials with the aid of the Mixed-Solute-Exclusion Method in conjunction with the solution of the Fredholm equation. Experimentally-determined distribution coefficients of solutes in several porous glasses (systems with prior known porous structures) were used to calculate the pore-size distribution. Our results exhibit good agreement with the experimental data, even for bimodal pore structures.

These initial studies to verify the practicability of the Mixed-Solute-Exclusion Method were accompanied by first preliminary experimental studies for a polyelectrolyte hydrogel. The preliminary results are encouraging but further efforts are required to reduce experimental uncertainties. These efforts are now in progress.

Experimental investigation of the AAm/MAPTAC hydrogel with two different probe-solute series (Dextran and Poly (ethylene glycol/oxide)) yielded two different pore-size distribution with mean diameters of 84 Å and 186 Å. This significant difference was due to a deterioration of the chromatographic columns during our measurements which resulted in erronous determination of the probe-solute concentrations. This source of experimental error is now corrected and therefore it is likely that subsequent experimental results will be of much better quality.

2. Introduction

A gel is a cross-linked polymer network in a liquid medium. Its properties depend strongly on the polymer-liquid interaction. The liquid prevents the polymer network from collapsing into a compact mass, and the network, in turn, retains the liquid. When the liquid is water, the cross-linked polymer is a hydrogel which swells sometimes very strongly. When the network is a polyelectrolyte, the degree of swelling depends on temperature, pH and salt concentration but mostly on the water-polymer interaction.

Because of these properties some applications of these gels have been investigated and developed. Well-known applications include contact lenses, electrophoresis media and chromatographic packings. But there exists a potential for other applications such as the use of gels in chemomechanical systems, controlled-drug release and in biochemical and organochemical separations.

To develop and design hydrogels for applications, it is important to characterize the gel as a function of gel chemistry and composition. Gel characterization involves determination of swelling equilibria and kinetics, investigation of mechanical behavior and analysis of gel microstructure.

Methods for measuring gel microstructure are different from common methods such as mercury porosimetry or nitrogen adsorption because gels are swollen in a liquid medium; therefore, pores are not accessible to mer-

cury or nitrogen. We use here a solute-exclusion method for determining the microstructure, in particular, pore sizes and pore-size distributions.

Solutions with certain solutes at known concentrations, which cover a wide range of molecular weight range, are brought into contact with the hydrogel. Due to the porous structure of the hydrogel, some solutes migrate into the gel; others do not. The differences in concentrations of each solute is measured by means of Gel Permeation Chromatography (GPC). These differences are subsequently used for estimating pore sizes and pore-size distributions.

We use two different kinds of probe-solutes: one set of solutions with Dextrans- and Oligosaccharides and the other set with Poly (ethylene glycols), Poly (ethylene oxides) and Ethylene glycol. The reason for using two different series of probe solutes is to investigate the influence of different porbes on measured pore-size distributions.

In this work, we prepared a polyelectrolyte hydrogel containing acrylamide (AAm) copolymerized with the cationic (3-Methacrylamidopropyl) trimethylammonium chloride (MAPTAC). To obtain a network structure, we added N,N'-methylenbisacrylamide (BIS) as a crosslinking agent.

To our best knowledge, the only structural analysis of a hydrogel by size-exclusion (SE) was performed by Kuga /1,2/. The experimental procedure used in our work is based on that used by Kuga. However, the analysis for obtaining pore-sizes and pore-size distributions is different from that of Kuga. We use a special numerical procedure for solving the Fredholm-Equation, a type of integral equation. This integral equation transforms the experimentally-determined distribution of the solutes between the liquid phase and the gel phase to a theoretically-based pore-size distribution.

We present in this paper the swelling equilibria, distribution coefficients and the pore-size distribution of the AAm/MAPTAC-hydrogel. The results have to be regarded preliminary due to imperfect experimental conditions. However, initial studies have shown that a large increase in accuracy of the results can be obtained by optimizing the experimental procedure. Investigations using the improved method are under way; details are discussed in Chapter 6.

3. Experimental Section

3.1. Probe Solutions

Solutes used to investigate the pore structure of hydrogels should meet the following requirements:

- Good solubility in water
- No specific interaction with the gel matrix (adsorption, electrostatic interactions, etc.)
- Sufficiently monodisperse fractions covering a large MW-range
- Well-defined size, which does not change significantly inside the gel matrix

Globular molecules, such as proteins, would be the optimum probe solutes with respect to a well-defined size. Proteins are also monodisperse, however, we do not use tehm because they bear charged groups which interact strongly together and with the gel matix. Even if we used a pH corresponding to the isolelectric point, the protein would still have significant electric moments.

Regarding all requirements, the best choice for probe solutes soluble is:

1. Aqueous Dextran-/Oligosaccharide solutions

2. Aqueous Poly (ethylene glycols)/ Poly (ethylene oxides)/ Ethylene glycol solutions

Dextran polymers were provided by Sigma Chemical Co., St. Louis, MO 63178, U.S.A., and by Pharmacia LKB, Uppsala, Sweden. Poly (ethylene oxides) were supplied by Aldrich Chemical Co., Milwaukee, WI 53201, U.S.A., Poly (ethylene glycols) by Union Carbide Co., Danbury, CT 06817, U.S.A., and Ethylene Glycol by Fisher Scientific, Fairlawn, NJ 07410, U.S.A..

Kuga /1/ described three different methods of solute exclusion: Single-point-SE, Column-SE and mixed-SE. In single-point-SE method solutions with only one probe solute is used and brought into contact with the gel of interest. Although this method is a strongly time-consuming procedure due to many different solutions, there is no need for any separation process (for example chromatography) to separate the probe solutes. In contrast to this method the mixed-SE method uses only one solution comprising different probe solutes which cover a wide range of molecular weight. According to this method, the experiments have to be carried out by means of a separation process coupled with a detection system. The column-SE method is a dynamic version of SE, where the column is packed with the hydrogel. Although this method saves much time and amounts of expensive polymer-standards, it is only applicable to gel samples which are available in the form of rigid and finely divided particles.

We perform our experiments using the mixed-SE method, but we use 3 or 4 different solutions, each containing three probe solutes for the Dextran series and the Poly (ethylene glycol/oxide) series, respectively. Only the first aqueous Poly (ethylene glycol/oxide) mixture contains two probe solutes. The split into 3 or 4 different solutions was necessary due to the re-

solving power of the existing chromatographic equipment. The compositions of the solutions are given in Table 1 and 2.

Solution 1		Solution 2		Solution 3	
Solutes	wt-%	Solutes	wt-%	Solutes	wt-%
Dextran 2.000.000	0.16	Dextran 500.000	0.15	Dextran 150.000	0.2
Dextran 70.000	0.2	Dextran 40.000	0.15	Dextran 11.000	0.1
Raffinose	0.04	Glucose	0.04	Succrose	0.04

Table 1. Composition of the Dextran solutions

Solution 1		Solution 2		Solution 3		Solution 4	
Solutes	wt-%	Solutes	wt-%	Solutes	wt-%	Solutes	wt-%
PEG 200	0.8	PEG 300	0.7	PEG 400	0.7	EG	1.0
		PEG 8000	0.4	PEG 8000	0.4	PEG 3350	0.4
PEO 100.000	0.25	PEO 600.000	0.25	PEO 900.000	0.25	PEO 4.000.000	0.16

Table 2. Compositions of the Poly (ethylene glycol/oxide) solutions

3.2. Gel samples

The hydrogel in this work is a polyelectrolyte AAm/MAPTAC gel cross-linked with BIS with the following composition:

$$\%T = \frac{\text{mass of all monomers (g)}}{\text{volume of water (ml)}} \times 100 = 15\%$$

$$\%C = \frac{\text{moles of BIS in feed solution}}{\text{total moles of monomer in feed solution}} \times 100 = 0.5\%$$

$$\%MAPTAC = \frac{\text{moles of MAPTAC in feed solution}}{\text{total moles of monomer in feed solution}} \times 100 = 3\%$$

Synthesis of this hydrogel is described in /3/.

The gel samples were swollen in purified and filtered water, provided by a Barnstead Nanopure II System. The water was changed every day and weighing measurements were performed to monitor the swelling behavior. After eight days, swelling-equilibrium was reached; the swelling capacity was then determined to be 85 (swollen gel (g) /dry gel (g)), which is in good agreement with previous experimental data /4/.

3.3. Chromatographic Equipment and Attached Devices

Since we have solutions with more than one probe solute, it is necessary to separate the solutes and subsequently to detect them. The heart of the chromatographic apparatus consists of two HPLC gel filtration columns, a Bio-Gel TSK-30 and a Bio-Gel TSK-40 column (300mm x 7.5mm) purchased from Bio-Rad, Richmond, CA 94804, U.S.A.. The mean pore sizes are 250 and 500Å respectively, and the separation ranges in molecular weight for Poly (ethylene glycols) are 1.000-40.000 g/mol and 2.000-400.000 g/mol, respectively. The columns are operated at a constant temperature of 35°C, equipped with a column heater and a temperature control unit purchased from Rainin Instrument Co., Woburn, MA 01801, U.S.A..

Deionized, filtered and degassed water was pumped at a flow-rate of 0.8 ml/min (±1%) by a computer-operated one-piston pump consisting of a drive module and an interchangeable pump head. An additional pressure monitor displays the actual inlet pressure and turns off the pump automatically if the high- or the low-pressure limit is reached; these limits are set by the operator. The pump and the monitor are also provided by Rainin Instrument Co..

The solutions were injected by means of a syringe-loading-sample injector, model No.7125, equipped with a 200µl sample loop, supplied by Rheodyne Incorporated, Cotati, CA 94928, U.S.A..

The different probe solutes, eluted through the HPLC columns, were detected by a differential refractometer, No. 731.88, Wissenschaftliche Gerätebau Dr.-Ing. Herbert Knauer GmbH, Berlin, Germany. Since the refractive index of liquids depends strongly on temperature, the flow-cell of the refractometer is maintained at a constant temperature by an external temperature controller. The obtained data points were transfered through an interface to an IBM personal computer for analysis of the peak areas and peak heights. The software used for collecting, processing and reprocessing the data is a program package called Nelson Analytical 3000 Chromatography System (updated version 4.1), purchased from Nelson Analytical Inc., Cupertino, CA 95014, U.S.A

3.4. Experimental Procedure

First, the stock solutions were chromatographed at least three times. Then several beakers were filled with each five gel samples of an approximate weight of 12 g (swollen state). We chose three different amounts of the solutions to be added to the gel samples; the ratios of solution (g) / swollen

gel (g) were about one, two and three. We did not have any prior knowledge of the structure of the hydrogels and we wanted to have a decrease of the concentrations of about 50%. Therefore, we selected three different ratios to obtain measurable concentration differences.

The filled beakers were transfered to a temperature-controlled bath, purchased from Blue M Electric, Blue Island, IL 60406, U.S.A., Model MSB-3222A-1, at a constant temperature of 25° C and shaked at a moderate frequency, until swelling equilibrium was reached. Weighing measurements were performed every day for monitoring the swelling behavior of the gel samples in the different solutions. After equilibrium was reached, the gel samples were separated from the equilibrated solutions, thoroughly washed and subsequently dried. The remaining equilibrated solutions were first filtered (Whatman filter paper no. 40) to remove gel particles which would affect the chromatographic measurements. After filtering, the equilibrated solutions and the corresponding stock solutions were alternately chromatographed at least three times. This procedure of alternate measurements of stock solution and equilibrated solution was necessary to obtain accurate chromatographic results, since slight changes of the GPC-equipment (state of the column, temperature, state of the mobile phase) greatly affect the results. The differences in concentrations of each probe solute were used to calculate the distribution coefficient and the pore-size distribution.

4. Analysis and Theoretical Models

4.1. Principle of the Mixed-Solute-Exclusion Method

In the following section we denote all quantities which change during the experiment with one prime (′) before contacting the probe solutions and the gel samples. We use a double prime (″) for quantities at equilibrium (after contacting).

The masses of the gel samples (m'_{GS}) in the swollen state consist of the cross-linked polymer network (m_{PN}), the imbibed liquid ($m'_{Liq.,imb.}$) and excess-liquid ($m_{Liq.,exc.}$), which sticks to the surface of the gel samples:

$$m'_{GS} = m_{PN} + m'_{Liq.,imb.} + m_{Liq.,exc.} \qquad (4.1.-1)$$

Contacting the probe solutions with the gel samples results in an initial uneven distribution of probe solutes in the entire system (gel plus solution). This gives rise to an increase of osmotic pressure outside the gel. Two mechanisms tend to decrease the osmotic pressure difference between the gel phase and the outer solution phase. Migration of some molecules into the gel reduces the pressure difference by yielding a more uniform distribution of solutes. The remaining osmotic pressure difference causes the gel to expel water to dilute the surrounding solution. Therefore, swelling of the gel in equilibrium with the probe solutions gives:

$$m''_{GS} = m_{PN} + m''_{Liq.,imb.} \qquad (4.1.-2)$$

The imbibed liquid, in turn, may be split into two fractions: One fraction ($m''_{acc.}(M)$) is accessible to the solutes of molecular weight M while the remaining fraction ($m''_{non-acc.}(M)$) is not affected by the solute molecules:

$$m''_{Liq.,imb.} = m''_{acc.}(M) + m''_{non-acc.}(M) \qquad (4.1.-3)$$

The difference between the initial imbibed liquid ($m'_{Liq.,imb.}$) and the equilibrated imbibed liquid ($m''_{Liq.,imb.}$) represents the expelled water ($\Delta m_{Expelled}$):

$$\Delta m_{Expelled} = m'_{Liq.,imb.} - m''_{Liq.,imb.} \qquad (4.1.-4)$$

The modified swelling capacity of the gel samples, which is caused by the osmotic pressure, results in an alteration of the concentration of the probe solutes in the surrounding solution phase. The initial weight concentration (w'(M)) is the amount of probe solute ($m_{P-solute}(M)$) divided by the mass of pure solvent ($m_{Solv.}$). Since the total weight concentrations of probe solutes in solution is about 1%, we neglect the relatively small amount of the total mass of probe solutes:

$$w'(M) = \frac{m_{P-Solute}(M)}{\sum m_{P-Solutes} + m_{Solv.}} \sim \frac{m_{P-Solute}(M)}{m_{Solv.}} \qquad (4.1.-5)$$

As a result of solutes penetrating into the gel and migration of imbibed liquid out of the gel into the liquid phase, the concentration w'' is modified:

$$w''(M) = \frac{m_{P-Solute}(M)}{m_{Solv.} + m''_{acc.}(M) + \Delta m_{Expelled} + m_{Liq.,exc.}} \qquad (4.1.-6)$$

The dilution ratio is the equilibrium concentration divided by the stock concentration:

$$\frac{w''(M)}{w'(M)} = \frac{m_{Solv.}}{m_{Solv.} + m''_{acc.}(M) + \Delta m_{Expelled} + m_{Liq.,exc.}} \qquad (4.1.-7)$$

Combination with equations (4.1-1) to (4.1.-4) yields:

$$m''_{non-acc.}(M) = m'_{GS} - m_{PN} + \left[1 - \frac{w'(M)}{w''(M)}\right] \cdot m_{Solv.} \qquad (4.1.-8)$$

The dilution ratio $\frac{w'(M)}{w''(M)}$ is determined by gel chromatography. The other quantities m'_{GS}, m_{PN} and $m_{Solv.}$ are measured by weighing and thus we obtain the amount of non-accessible liquid as a function of molecular weight M. If the relationship between the molecular weight M and the molecular radius r is known, $m''_{non-acc.}(M)$ can be converted into $m''_{non-acc.}(r)$, which is interpreted as the cumulative pore-size distribution of the gel sample /1/.

The final equation (4.1-8) represents the **Solute- Exclusion curve (SE-curve)** which provides valuable information about the quantity of non-accessible water of a probe solute within the gel as a function of probe-solute radius. This functional relationship used to be regarded as the cumulative pore volume of the gel. However, identification of the SE-curve with the pore-size distribution is not correct /2/, as is now well known. It would mean that all the liquid existing in pores greater than the molecular size of a solute is available as a solvent for the solute, or alternatively that the center of gravity of a solute molecule can migrate throughout within the accessible pores with equal probality. This is obviously wrong as long as the solute has a finite volume. This excluded- volume effect is shown in Fig 1. and known as the Wall Effect /6/. The important Wall Effect is considered in this work, which converts the SE curve as a function of solute radius into the pore-size distribution as a function of pore radius (see following Chapter).

Solute sizes are given by the Stokes radius, radius of gyration, root-mean-square average end-to-end distance and hydrodynamic volume. The hydrodynamic volume has been accepted as a general size parameter (see the

various references in /5/). Table 3 gives experimentally-determined relationships between the molecular weight and the hydrodynamic radius r of a polymer in a particular solvent /5/. Table 4 shows calculated hydrodynamic radii for the probe solutes used in this work:

Solute	r_h (Å)
Dextran	$0.271 \cdot M^{0.498}$
Poly (ethylene glycol)	$0.255 \cdot M^{0.517}$
Poly (ethylene oxide)	$0.166 \cdot M^{0.573}$

Table 3. Relationships between molecular weight and hydrodynamic radius in water

Here M is the molecular weight corresponding the peak volume, M_p. Thus, unless M_p is stated by the supplier, the elution volume of polydisperse samples corresponding to M_n or M_w must be evaluated /5/.

Dextran, Oligosacch.	r_h (Å)	Poly (ethylene glycol/oxide)	r_h (Å)
D 2.000.000	372	PEO 4.000.000	1007
D 500.000	187	PEO 900.000	428
D 150.000	102	PEO 600.000	340
D 70.000	70	PEO 100.000	122
D 40.000	53	PEG 8000	27
D 11.000	28	PEG 3350	17
Raffinose	6	PEG 400	6
Sucrose	5	PEG 300	5
Glucose	4	PEG 200	4
		Ethylene Glycol	2

Table 4. Calculated hydrodynamic radii for probe solutes

The experimental distribution coefficient is the ratio of the difference between the maximum non-accessible amount of imbibed liquid (size-exclusion limit, $m_{non.,acc.,\infty}$) and the amount of non-accessible imbibed liquid of the solute to the former amount:

$$K(M) = \frac{m_{non.,acc.,\infty} - m_{non.,acc.}(M)}{m_{non.,acc.,\infty}} \qquad (4.1.-9)$$

The maxiimum amount of imbibed liquid is determined by polymers of high molecular weight which cannot migrate into the gel structure; therefore, the imbibed liquid in the gel structure is not accessible to these polymers.

Smaller polymers penetrate into the network more or less and cause an exchange of imbibed liquid and solute molecules. The smallest probe solutes may occupy almost the entire amount of imbibed liquid; therefore, the amount of non-accessible liquid within the gel is very small. Fig. 2 represents this relationship qualitatively.

4.2. Theoretical Models

In this work, two theoretically-based models are used: on the one hand, the **Random-Spheres-Model (RSM)** for corroborating the experimentally-determined distribution-coefficient and on the other hand, the **Brownian-Motion-Model (BMM)** in conjunction with the mathematical solution of the **Fredholm-Equation**, which converts the experimental distribution coefficient into a theoretically- based pore-size distribution and takes into account the previously described **Wall Effect**. A short description of these models is given here. Further information is given in /7, 8, 9/.

4.2.1. The Random-Spheres-Model (RSM)

The RSM-Model was introduced by Weissberg /7/, but Van Eekelen /8/ provided the extension of this model by introducing a distribution function for the microspheres and the derivation of the calculation of pore-size distributions. Utilization and corroboration of this extended RSM-Model is discussed by Van Krefeld and Van Den Hoed /9/.

In general, distribution coefficients of solutes between an outer phase and a porous material (inner phase) provided by theoretical models are only meaningful if prior information about the size of the solutes and the structure of the porous material (=pore-sizes) are available. Such information is required because of interactions between the solutes and the porous mate-

rial. However, the purpose of this paper is to determine the pore-size distributions; the required information is not available.

The Random-Spheres-Model (RSM) avoids these difficulties by a statistical treatment of a large number of microscopic solid bodies, which allows a simulation of a porous structure.

In its simplest form, the RSM is constructed by placing a certain number, n, of identical solid microspheres of radius S_o in a volume V, without any correlation between the positions of the spheres. This procedure generates a structure, where some microspheres remain isolated and others overlap. The pore space is constituted by the interstices between the microspheres. Fig. 3 indicates such a configuration with 150 microspheres. The values of n and S_o are chosen in such a way that the real specific void fraction Ψ and the specific surface area Σ are obtained.

An extension of this model was performed by introducing a distribution function of the microspheres f(S) to obtain a more realistic porous structure /8/:

$$\int_0^\infty f(S)dS = 1 \qquad (4.2.1.-1)$$

S Radius of microspheres

f(S) Distribution function of microspheres

The fundamental equations of the RSM are based on a statistical treatment for the microspheres /7/:

$$V = \log \Psi \qquad (4.2.1.-2)$$

$$S_o = -\frac{3\Psi}{\Sigma} \log \Psi \qquad (4.2.1.-3)$$

V	Total specific volume (per unit volume)
S_o	First moment of the distribution function f(S)
Ψ	Void fraction
Σ	Specific surface area (per unit surface area)

For a porous material with a void fraction Ψ, we define the reduced void fraction $\Psi'(r)$ as the volume accessible to a point particle which has to stay at least a certain distance away from the solid surface. Thus, $\Psi'(r)$ is the volume accessible to the center of a spherical particle of radius, r, and it is found from equations (4.2.1.-1) and (4.2.1.-2):

$$\frac{\log \Psi'(r)}{\log \Psi} = \int_0^\infty f(S)\left(\frac{S+r}{S}\right)^3 dS \qquad (4.2.1.-4)$$

$$\frac{\log \Psi'(r)}{\log \Psi} = 1 + 3rL_1 + 3r^2L_2 + r^3L_3 \qquad (4.2.1.-5)$$

$$L_n = \int_0^\infty \frac{f(S)}{S^n} dS, \qquad L_1 = \frac{1}{S_o}$$

The concept of a reduced void fraction $\Psi'(r)$ for particles of radius r, may also be used to define a pore-radius-distribution f(R) within the RSM /8/.

First consider a "Random-Pores-Model" with the same void fraction Ψ, in which the pore volume consists of randomly overlapping pores. The pore-radius-distribution function f(R) is defined as:

$$\int_0^\infty f(R)dR = 1 \qquad (4.2.1.-6)$$

If we require that the reduced void fraction in this "Random-Pores-Model" is the same function $\Psi'(R)$ of R as in the RSM, we obtain an equation which uniquely determines f(R):

$$\int_0^\infty f(R)\left(\frac{R-r}{r}\right)^2 dR \qquad \int_0^\infty f(S)\left(\frac{S+r}{S}\right)^3 dS \qquad (4.2.1.-7)$$

$$(1-\Psi) \qquad = 1-\Psi$$

For any given f(S) and Ψ, this equation for f(R) is solved by taking the logarithm of both sides and differentiating three times with respect to r. The resulting equation is:

$$f(x) = -\frac{e^{-Q}\,x^2}{2R_o \ln(1-\Psi)}\left[\frac{1+e^{-Q}}{(1-e^{-Q})^3}Q'^3 - \frac{3}{(1-e^{-Q})^2}Q'Q'' + \frac{1}{1-e^{-Q}}Q'''\right]$$

$$Q = (1 + 3x + 3x^2\frac{L_2}{L_1^2} + x^3\frac{L_3}{L_1^3})\ln\frac{1}{\Psi}$$

$$x = \frac{R}{S_o} \qquad Q' = \frac{dQ}{dx} \qquad Q'' = \frac{dQ^2}{d^2x} \qquad Q''' = \frac{dQ^3}{d^3x} \qquad (4.2.1.-8)$$

The distribution coefficient is the ratio of the volume of pores accessible to the centre of mass of the molecules ($V_{P,acc.}$) to the total volume of the pores ($V_{P,tot.}$):

$$K = \frac{V_{P,acc.}}{V_{P,tot}} \qquad (4.2.1.-9)$$

According to the RSM, the distribution coefficient K is defined:

$$\Psi' = \frac{V_{P,acc.}}{V_{Ges.}} \qquad \Psi = \frac{V_{p,tot.}}{V_{Ges.}}$$

$$K = \frac{\Psi'}{\Psi} = \frac{1}{\Psi}e^{(1+3rL_1+3r^2L_2+r^3L_3)\ln\Psi} \qquad (4.2.1.-10)$$

We have chosen three different distribution functions for the microspheres, a Delta function, a Gaussian and a bimodal Gaussian , which were used to calculate pore-size distributions and distribution-coefficients. Results using this RSM model are shown in Chapter 5.

4.2.2. Brownian-Motion Model

This model was mainly developed by Casassa et al /10-12/ to obtain an equilibrium theory for exclusion chromatography of branched and linear polymer chains. This model represents an extension of the "Random-Spheres-Model", which treats the solute molecules as rigid spheres.

First, we have some assumptions:

1. The solution is dilute; we neglect solute-solute interactions.

2. The polymer-solvent combination is at the Flory temperature† , that means $T = \Theta$, and hence the polymer chain behaves like an unperturbed chain.

3. We have no adsorption of polymer on void surfaces.

4. We assume polymer-solvent interactions are not altered in the neighborhood of these surfaces relative to what they are in the bulk.

These assumptions allow us to describe the molecular conformations of flexible polymer chains by random-flight statistics.†† Furthermore, the dis-

---

† From a physical point of view, the Θ -point arises because of the apparent cancellation at this temperature of the effect of volume exclusion of the segments, which tends to enlarge the molecule, and the effect of van der Waals attractions between segments, which contract the molecule.

†† Random flight: A particle undergoes a sequence of displacements $\vec{r}_1, \vec{r}_2, \vec{r}_3, \ldots \vec{r}_n$; the magnitude and direction of each displacement is independent of all preceding ones. This means a chain consisting of linkages of length l joined in a linear sequence has no restrictions on the angles between the bonds, only the bond length is fixed. Such a chain is a "freely-jointed chain". The configuration of the freely-jointed polymer chain resembles the path described by a diffusing particle such as a gas molecule. A free path of a gas molecule corresponds to a bond vector. This chain configuration problem, reduced in this manner, is called the random flight problem.

tribution of polymers between the outer phase and the voids is determined entirely by the loss of conformational entropy attendant on the transfer of a chain from the outside to the limited space within the void.

To calculate the change in conformational freedom, we may begin by seeking a solution, consistent with appropriate boundary conditions, of the following differential equation, which is formally identical to the diffusion equation:

$$\frac{\partial P_n(x,y,z)}{\partial n} = \frac{b^2}{6} \nabla^2 P_n(x,y,z) \qquad (4.2.2.-1)$$

$P_n(x,y,z)dxdydz$ Probability for finding the n-th step (or chain segment) of a random flight within a volume element dxdydz at a point labeled by a vector $\vec{r}$, drawn from the origin of the coordinate system.

b^2 Mean-square step length.

The boundary condition requires that each $P_n(x,y,z)$ vanishes at every point on the boundary of the cavity. Fig. 4 shows the number of conformations available to a two-step polymer in one dimension which are reduced in the case of a boundary from the value 4 to 3. For the idealized conditions assumed , the fraction of conformations remaining available to the chain confined by the void is just the partition coefficient. The partitioning is the equilibrium ratio of the concentration of a polymer species per unit volume of void space to that in the outer phase.

The problem of solving the diffusion equation is very similiar to problems in heat conduction. Solutions exist and we only focus on the results. We can thus obtain explicit relations for the distribution coefficient K in terms of the mean-square radius $r^2 = Nb^2/6$ (N = Number of steps) of the unconfined linear polymer chain and the dimensions of the cavity. Three different

geometries were introduced by Cassasa et al /10-12/: a sphere with radius R, a cylindrical cavity of radius R and infinite length, and finally, a slab-shaped cavity between two planes of indefinite extent separated by a distance 2R. We have the following functions for calculating the distribution coefficient:

$$K_{Sphere} = \frac{6}{\pi^2} \sum_{m=1}^{\infty} \frac{1}{m^2} e^{-(m\pi \frac{r}{R})^2} \qquad (4.2.2.-2)$$

$$K_{Cylinder} = 4 \sum_{m=1}^{\infty} \frac{1}{\beta_m^2} e^{-(\beta_m \frac{r}{R})^2} \qquad (4.2.2.-3)$$

where β_m are the roots $J_o(\beta) = 0$, J_o indicating a Bessel function of the first kind and zero order.

$$K_{Slab} = \frac{8}{\pi^2} \sum_{m=0}^{\infty} \frac{1}{(2m+1)^2} e^{-(\frac{(2m+1)\pi}{2} \frac{r}{R})^2} \qquad (4.2.2.-4)$$

When $\frac{r}{R} > 0.1$, these series converge rapidly. One remarkable advantage of htese results is that there are no adjustable parameters.

4.3. Pore-Size Distribution

The distribution coefficient is defined as the concentration of a solute in one phase divided by the concentration of this solute in the other phase. In the particular case of a solution containing dissolved solutes in equilibrium with a hydrogel, the distribution coefficient is the concentration ratio of each solute in the gel phase to the coexisting solution phase:

$$K(r) = \frac{w''_{Gel}}{w''_{Solution}} \qquad (4.3.-1)$$

The concentration in each phase is the amount of solute divided by the amount of solvent present in each phase:

$$w''_{Gel} = \frac{m_{Solute}}{m_{Solv.,P-tot.}} \qquad (4.3.-2)$$

$$w''_{Solution} = \frac{m_{Solute}}{m_{Solv.,Solution}} \qquad (4.3.-3)$$

At equilibrium, the partitioning solute has reached a uniform distribution in the solution phase and in the particular part of the gel phase which is accessible to the solute. In other words, the concentration in the accessible part of the gel phase is the same as that in the solution phase. This latter statement holds only if steric effects (= size exclusion) are responsible for the migration of solutes into the pores of the gel. Any other specific interactions are neglected here; these interactions would cause an uneven concentration profile in the solution-gel(accessible) phase system. Therefore we can recast the expression for the concentration of the solute in the solution phase in the following way:

$$w''_{Solution} = \frac{m_{solute}}{m_{Solv.,P-acc.}} \qquad (4.3.-4)$$

With equation (4.3.-1) we obtain the following expression for the distribution coefficient (see Fig. 5):

$$K(r) = \frac{m_{Solv.,P-acc.}}{m_{Solv.,P-tot.}} = \frac{V_{P-acc.}(r)}{V_{P-tot.}} \qquad (4.3.-5)$$

In other words, the distribution coefficient of a solute is the ratio of the accessible pore volume to the total pore volume.

In the literature, the definition of the pore-size distribution has been used in several ways. However, it has not always been applied in the right way;

often, previous authors have neglected the distinction between the cumulative and the differential pore-size distribution. The proper definition of the pore-size distribution is used here, as shown below.

The differential pore-size distribution is denoted by f(R) and defined in the following way:

$$\frac{dV}{V_{P-tot.}} = f(R) \cdot dR \qquad (4.3.-6)$$

f(R) dR represents the fraction of the total pore volume containing pores with radii between R and R + dR. The integration of equation (4.3.-6) yields the cumulative pore-size distribution g(R):

$$\frac{1}{V_{P-tot.}} \int_0^V \tilde{dV} = \int_0^R f(\tilde{R}) d\tilde{R} \qquad (4.3.-7)$$

$$g(R) = \int_0^R f(\tilde{R}) d\tilde{R} \qquad (4.3.-8)$$

g(R) gives the fraction of the total pore volume containing pores with radii ranging from 0 to R.

For any group of pores of radii between R and R + dR with a total volume dV the fraction of the volume accessible to a molecule of radius r is given by:

$$K(R,r) = \frac{dV_{P-acc.}(r)}{dV} \qquad (4.3.-9)$$

$dV_{P-acc.}(r)$ is the pore volume with pores of radii between R and R + dR accessible to a molecule of radius r. Thus the amount of accessible volume for this group of pores is:

$$dV_{P-acc.}(r) = K(R,r) \cdot dV \qquad (4.3.-10)$$

$$dV_{P-acc.}(r) = K(R,r) \cdot f(R) \cdot V_{P-tot.} \cdot dR \qquad (4.3.-11)$$

The total accessible volume for a solute molecule with radius r for all groups of pores leads to the integration of equation (4.3.-11):

$$\int_0^{V_{P-acc.,\infty}} \frac{dV_{P-acc.}(r)}{V_{P-tot.}} = \int_0^{R_\infty} K(R,r) \cdot f(R) \cdot dR \qquad (4.3.-12)$$

The integration of the left hand side results in the overall distribution coefficient K(r) in accordance with equation (4.3.-5):

$$K(r) = \int_0^{V_{P-acc.,\infty}} \frac{dV_{P-acc.}(r)}{V_{P-tot.}} = \frac{V_{P-acc.}(r)}{V_{P-tot.}} \qquad (4.3.-13)$$

To obtain the differential pore-size distribution, the final equation to evaluate the experimental data is given by:

$$K(r) = \int_0^{R_\infty} K(R,r) \cdot f(R) \cdot dR \qquad (4.3.-14)$$

The left-hand side represents the measured overall distribution coefficient as a function of molecular radius r. The right-hand side consists of the differential distribution coefficient as a function of r and R and the desired pore-size distribution f(R). The differential distribution coefficient K(R,r) is provided by the Brownian Motion Model (see previous Chapter). Solving the integral-equation (4.3.-14) to obtain f(R) is a serious problem. This equation is well-known as the inhomogeneous Fredholm-equation of the first kind (see Appendix).

5. Results and Discussion

5.1. Theoretical Results

To date, the only hydrogel studied with the mixed-SE method is Sephadex G-100† (Kuga /1,2/). This investigation is important for our studies because we are able to compare our experimental results with those of Kuga. Additionally, we have used his experimental results to obtain the "true" pore-size distribution, that is, with consideration of the Wall Effect described earlier. Furthermore, we have utilized many experimental data of rigid porous materials of either known or measured pore sizes to compare our theoretically-obtained pore-size distribution with these experimental data.

The Random-Spheres Model

Fig. 6 and 7 show the calculated RSM distribution coefficient with the experimental data of Kuga of the PEO/PEG and Dextran series, respectively. The void fraction Ψ was calculated to be 0.69 by using the experimental obtained void-volume V_0 and the total volume $V_0 + V_i$ according to the column method performed by Kuga. Since no data of the mass of the swollen gel and the dried gel are mentioned in /1,2/, this is the only way to obtain Ψ. The only adjustable parameters are the mean values of the different distribution functions of the microspheres and the variances for the Normal distribution and the Bimodal distribution. Since the influence of the vari-

---

† Sephadex is a cross-linked Dextran gel, which was invented by Porath and Florin in 1959

ance on the results is small, we have set the variance to 4 and have only adjusted the mean values RDEL for the Delta function, RNORM for the Normal distribution and RNORM1 and RNORM2 for the Bimodal distribution. The calculated distribution coefficient is in good agreement with the experimental data, even though there exists a difference between the PEO/PEG and the Dextran series, which is caused by different experimental cumulative pore-volume data measured by Kuga. Both limiting values of inaccessible water (i.e. for very small and for very big solutes) agree very well, but the two cumulative pore-volume curves do not coincide; they are shifted apart with respect to the solute radius. The influence of the different distribution functions of the microspheres is very slight.

Figs. 8 and 9 show the calculated RSM pore-size distribution of Sephadex G-100. The mean pore radius for the PEO/PEG series is about 55 Å for the Delta function and the Normal distribution and about 50 Å for the Bimodal distribution function. Here the influence of the microspheres distribution on the resulting pore-size distribution is more significant than in the case of the distribution coefficient. The resulting pore-size distribution for the Dextran series shows a maximum of about 122 Å, which is a considerable deviation from the pore-size distribution obtained with the PEO/PEG series. In turn, this is caused by the different cumulative pore-volume curves. Kuga concluded in his paper that the difference between the two probe solute series is not significant. But he regarded the cumulative pore volume as a pore-size distribution, which is not correct.

Figures 10-15 show the calculated RSM distribution coefficients and the experimental distribution coefficients for various porous materials like Styragel and Merckogel /13,14/ ranging in mean pore radii from 17.5 Å to 500 Å. A serious limitation of the RSM-Model is its application to porous materials with a wide range of pore sizes, as one can see especially in

Figs.14 and 15. It is impossible to represent the experimental data in a proper way. The randomly-generated structure consists only of pores which have a more-or- less Gaussian pore-radius distribution. For example, Merckogel SI 100 has pores whose radii differ by an order of magnitude or more; this pore structure cannot be well represented by the RSM-Model.

The Brownian-Motion Model

To prove validity of the Brownian-Motion Model, it is necessary to have information about pore sizes, mean pore diameter or pore-size distributions because this model accounts for both the size of the solutes and the size of the pores. But the latter is exactly the information we want to obtain. Hence this model is only applicable for determining pore-size distributions with the aid of experimental data, i.e. K(r).

Partitioning of solutes between the outer phase (solution phase) and the inner phase (porous structure) follows because polymers of all types exhibit the same dependence of the distribution coefficient on the ratio of r (the radius of the solute-molecules) to R (the radius of the pores):

$$K(r,R) = f(\frac{r}{R}) \qquad (5.1.-1)$$

A theoretical model was developed by Casassa /12-14/ to describe the distribution coefficient K(r,R) (see Chapter 4.2) and has been verified for many porous materials, where one has initial information about the structure of the material, for example porous glasses. Fig. 16 shows the distribution coefficient as a function of r/R for the three geometric cavities based on equations (4.2.2.-2 - 4.2.2.-4). The experimental data for various controlled

porous glasses ranging from average-pore diameters† of 84 to 517Å were measured by Haller /15/. Comparison between the three theoretical curves and the experimental data yields the slab cavity as the best geometric pore shape for a reasonable representation of the experimental data. To calculate the distribution coefficient with cylindrical-shaped pores, the roots β_m of the Bessel-function of the first kind and order zero were taken from Carslaw and Jaeger /17/. The good agreement between the experiment and theory confirms the validity of the theoretical framework developed by Casassa.

To check the Brownian-Motion Model concerning calculations of pore-size distributions in conjunction with the solution of the Fredholm equation, we have utilized many experimentally-determined distribution coefficients of various porous materials with known pore structure. Figs.16-23 show the calculated pore-size distributions of several porous materials with known mean pore diameters. Those data were taken from Haller /15/, Yau et al /18/ and Gorbunov et al /19/. Agreement with experimental data is reasonable. Table 5 shows the calculated mean pore diameters of monodisperse and polydisperse porous glasses.

---

† The average-pore size of the controlled glasses determined by mercury- intrusion technique is defined as the pore diameter which was penetrated when half of the total volume available for mercury became filled /16/.

	Monodisperse				Polydisperse		
Porous glass(Å)	84	227	314	517	144 234	46 144 234 636	60 750
Calculated mean pore diameter(Å)	90	222	312	470	-	-	78 966
Deviation (%)	7.1	2.25	0.6	10.0	-	-	30.0 28.8

Table 5. Calculated mean pore diameters for several porous glasses.

The calculated pore-size distribution of the first two polydisperse porous glasses exhibit only one peak. Therefore, a comparison between the calculated and experimental mean pore diameter was not performed. An additional uncertainty occured because all these data were taken from graphs since no table with the exact measured data were available. Because of these circumstances the calculation of pore-size distributions with the Brownian-Motion Model is useful for obtaining reasonable results, especially for materials with a wide range of pore sizes. But regardless of these reasonable results, there is no possibility to prove the validity of this theory with experimental data for hydrogels. Because of this lack of data we must regard these calculations as no more than an estimate of pore-size distributions.

Figs. 24 and 25 show results of the calculation of pore-size distribution for Sephadex with the Brownian-Motion Model based on the measurements of Kuga with the PEG/PEO and Dextran probe solutes. 25. The resulting pore-size distributions for the two probe species are quite different; however, the two peaks are located in the same diameter range for both probe solute series. But still these results are not satisfactory regarding the influ-

ence of different probe species on the results. Unfortunately no PSD-data of Sephadex are available for comparing these poor results with the existing pore structure. Since no prior information of the pore-size distribution was used to solve the Fredholm equation, those results have to be regarded as an estimate. It is necessary to check further the influence of various parameters which can be set in the computer program to stabilize mathematically the solution of the Fredholm equation.

5.2. Experimental Results

Calibration of the Columns

Determination of the concentration ratio of the probe solutes is performed by size-exclusion chromatography. We have used two Bio-Rad TSK-columns with different pore sizes connected in series. To generate the various solutions with the different probe solutes which can be resolved with the existing chromatographic apparatus, it was necessary to carry out a calibration. Qualitatively, the objective of a calibration is to elucidate the order of elution of a group of solutes or, at least to define the feasibility of satisfactorily separating them /20/. Fig. 26 shows the calibration curve for both series of probe solutes (Dextran and PEO/PEG), that is, molecular weight (=solute radius) versus retention volume (=retention time x flow rate). As Fig. 24 indicates, no separation is possible in the high molecular weight ($\geq$ 100.000) range as well as in the low molecular weight ($\leq$ 400) range. But even the resolution of the two Dextran-solutes 70.000 and 11.000 is almost impossible, due to the polydispersity of these solutes and the band-broadening caused by eddy-diffusion, molecular diffusion and mass transfer /21/. Therefore the division into 3 and 4 solutions for the Dextran and the PEO/PEG series, respectively, was inevitable. The calibration curves of each probe solution for the Dextran and PEO/PEG series are shown in Fig

27 and 28, respectively. All show a linear relationship between the molecular weight and the retention time.

Solute-Exclusion Curve and Pore-Size Distribution

Fig. 29 shows the measured cumulative pore volume of the AAm/MAPTAC Hydrogel according to equation (4.1.-8) (page 13) for both series of probe solutes. The results for the Dextran-series are very poor, due to a deterioration of the resolving power of the GPC-apparatus. Thereafter, the columns were checked at Bio-Rad Research Laboratories; the TSK 40 column was worn out and not usable anymore. However, we believe we can obtain a similiar cumulative pore volume curve for the Dextran-series as for the PEO/PEG-series under the same experimental conditions;this has to be proved in further measurements.

The infinite non-accessible pore volume per gram of dry gel is about 79.4 (g/g dry gel), which we could measure for both probe solutes series. The measured swelling capacity of the gel samples in equilibrium is about 77.5 (g/g dry gel), which is in good agreement with the infinite non-accessible pore-volume. The non-accessible pore volume for very small probe molecules is about 20.7 (g/ g dry gel), which we could not measure for the Dextran-series. The peaks of the Oligosaccharides of the equilibrated solutions were not accurately detectable; therefore, the value of non-accessible pore volume has been set to zero, which, however, is not correct.

The distribution coefficients of both series are shown in Fig. 30. The experimental data are affected in the same way as described above, that is, we have deviations at the low radius range and good agreement at the high radius range. Based on these experimental data, we have calculated the PSD with the Brownian-Motion Model for both series, as shown in Figs. 31 and

32. We have not achieved the same PSD, however. The Dextran data exhibit a steep ascent from 30 to 80 Å and then level in the high molecular weight range. In this range, the PEO/PEG data are still rising, indicating that pore volume is still accessible for those probe solutes. Therefore, the PSD for the PEO/PEG series exhibits pores of diameters up to 400Å, whereas the PSD -range for the Dextran-series ends at about 130Å. This discrepancy is caused by the experimental difficulties described above but we believe that we are able to improve our measurements with a new set of GPC- columns to measure solute concentrations more accurately.

6. Conclusions and Future Work

The pore-size distribution of a AAm/MAPTAC hydrogel was investigated using the Mixed-Solute-Exclusion method introduced by Kuga. This method was further developed in this work by taking into account the Wall Effect by using the Cassasa's Brownian-Motion model. This enhancement of the model led to an inhomogeneous integral-equation, the Fredholm equation.

We have utilized many published-experimental data for porous materials with known pore structure for comparing structural information obtained with the Brownian-Motion model and the known structure. The agreement is mostly reasonable, but sometimes poor, probalby due to experimental error in the reported data. These data were only available in terms of curves or graphs and not as tables with the exact measured data. However, the outcome of the Brownian-Motion model is remarkably better than that of the Random-Spheres model which was also examined in this work.

Unfortunately, the calculated pore-size distributions based on our measurements with two different probe solute series (Dextran and Poly (ethylene glycol/oxide)) are quite different. This difference in the pore-size distributions was attributed to a deteriotation of the GPC-columns during our measurements. However, these preliminary results show the feasibility of the Mixed-Solute Exclusion method to obtain information about porous structures of hydrogels. To increase accuracy, further improvements of the experimental procedure are under way; these include:

- Investigation of possibly dissolved charged gel particles in the equilibrated probe solutions, which affect the swelling equilibria significantly

- Minimization of mechanical stress on the gel samples (shaking, weighing) during the entire experiment to prevent the breakage of the hydrogels. Consequently, a new procedure for the determination of equilibrium has to be developed to replace of the present method of monitoring the swelling equilibria.

- The influence on the results of various mathematical input parameters to calculate the pore-size distribution by solving the Fredholm equation has to be determined. In particular, it is important to stabilize the ill-posed problem of the Fredholm equation (see Appendix 8.1) by choosing appropiate parameters.

- Investigations of the following kinds of hydrogels will be performed:

  1. AAm/MAPTAC hydrogels with 3% MAPTAC, 15% T and varying in cross-link density (C=0.2%, 0.5%, 1.0%)

  2. AAm/MAPTAC hydrogels with 3% MAPTAC, 0.5% C and varying in total amount of monomer (T=15%, 20%, 25%, 30%)

7. Acknowledgements

This work was supported by the Director, Office of Energy Research, Office of Basic Energy Sciences, Chemical Sciences Division of the U.S. Department of Energy under Contract Number DE-AC03-76SF00098. Michael Kremer is grateful to the DAAD for financial support through a fellowship. The authors would like to thank John Baker for synthesising the hydrogels; Alex Sassi and John Baker for helpful discussions; Chip Haynes for aid in in using the chromatographic apparatus; and Judy Lee and Jeannie Ahn who performed some of the measurements. Finally, the authors are greatly indebted to Wai-Kin Lam, Bio-Rad, for helping to maintain the GPC-columns and for fruitful discussions.

8. Appendix

8.1. Outline of the Solution of the Fredholm equation

The following paragraphs give a brief introduction of the solution of the Fredholm-equation. The computer-program CONTIN, which has been developed and maintained by Provencher /22-25/, was used to perform the calculations of the pore-size distributions.

Most experiments in the natural sciences are indirect. That is, the observed data, y_k, are related to the desired function or vector x by operators O_k:

$$y_k = O_k x + \varepsilon_k, \quad k = 1,....,n \qquad (8.1.-1)$$

where ε_k are unknown noise components. One is then faced with the inverse problem of estimating x from from the noisy measurements y_k. Often the O_k are approximated by linear integral operators, and in the case of calculating pore size distributions equation (8.1.-1) can be written:

$$K(r) = \int_0^{R_\infty} K(R,r) \cdot f(R) \cdot dR + \varepsilon(r) \qquad (8.1.-2)$$

The first step is to convert equation (8.1.-2) to a system of linear algebraic equations. This means to perform numerical integration of equation (8.1.-2):

$$K(r) = \sum_{m=1}^{N} c_m \cdot K(R_m,r) \cdot f(R_m) + \varepsilon(r) \qquad (8.1.-3)$$

c_m Weights of quadrature formula

With this converting step, it is assumed that errors in going from the integral equation to the system of algebraic equations are much less than $\varepsilon(r)$.Re-writing of equation (8.1.-3) yields the following equation:

$$K(r) - \varepsilon(r) = \sum_{m=1}^{N} c_m \cdot K(R_m,r) \cdot f(R_m) \qquad (8.1.-4)$$

$$y_k = \sum_{m=1}^{N} A_{m,k} \cdot x_m \qquad k = 1,....,n \qquad (8.1.-5)$$

n Number of measurements

or in vector style:

$$\vec{y} = \underline{A} \cdot \vec{x} \qquad (8.1.-6)$$

The integral form of the Fredholm equation is an ill-posed problem. The converting step from the integral to the system of algebraic equations converts this ill-posed problem to an ill-conditioned problem. This means that, even for arbitrarily small (but nonzero) noise levels in the K(r), there still exists a large (typically infinite) set S of solutions f(R) that all fit the K(r) within the noise level.

One member of S is the ordinary least squares solution of equation (8.1.-6), that means the set of x_m that satisfies

$$\sum_{k=1}^{n} w_k \left[\left[y_k - \sum_{m=1}^{N} A_{m,k} \cdot x_m \right] \right]^2 = \text{minimum} \qquad (8.1.-7)$$

or in vector style:

$$(\vec{y} - \underline{A}\vec{x}) \cdot (\vec{y} - \underline{A}\vec{x})' \cdot \underline{w} = \text{mininum} \qquad (8.1.-8)$$

w_k Weight function for least square method

To confine the set of possible solutions there exists a constrained regularized solution, which is the set of x_m that satisfies

$$\sum_{k=1}^{n} w_k \left[\left[y_k - \sum_{m=1}^{N} A_{m,k} \cdot x_m \right] \right]^2 + \alpha^2 \sum_{i=1}^{N_{reg.}} \left[\left[\sum_{m=1}^{n} L_{i,m} \cdot x_m \right] \right]^2 = \text{minimum}$$

or in vector style:

$$(\vec{y} - \underline{A}\vec{x}) \cdot (\vec{y} - \underline{A}\vec{x})' \cdot \underline{w} + \alpha^2 (\underline{L}\vec{x})'(\underline{L}\vec{x}) = \text{minimum} \qquad (8.1.-10)$$

The added term is called the regularizer. Its form is determined by specifying the matrix L. Its strength is determined by specifying α, the regularization parameter. If L is suitably chosen, the added term has a smoothing or stabilizing effect on the solution. For example, take $\underline{L}\vec{x} = (\vec{x})', (\vec{x})''$; if the k th derivation is selected, the process is termed k th order regularization.

9. References

/1/ Kuga, S. : Journal of Chromatography,**1981**,206,449-461

/2/ Kuga, S. : Journal of Chromatography Library-Volume 40,**1988** edited by P.L. Dublin, Chapter 6, 157-170

/3/ Hooper, H.H.; Baker, J.P.; Blanch, H.W.; Prausnitz, J.M. Macromolecules, **1990**,23,1096

/4/ Baker, J.P.; Acrylamide Copolymer Gels: Synthesis, Swelling, Microstructure. Master of Science Thesis, University of California, Berkeley,**1989**

/5/ Hagel, L. : Journal of Chromatography Library-Volume 40,**1988** edited by P.L. Dublin, Chapter 5, 119-155

/6/ Kubin, M. ; Vozka, S. : Journal of Polymer Science, Polymer Symposium, **1980**,68,209-213

/7/ Weissberg, H.L. : Journal of Applied Physics, 34,**1963**,2636

/8/ Van Eekelen, H.A.M. : Journal of Catalysis, 29,**1973**,75-82

/9/ Van Krefeld, M.E. ; Van Den Hoed, N.
Journal of Chromatography, 83, **1973**, 111-124

/10/ Casassa, E.F. ; Tagami, Y. : Macromolecules,2, **1969**, 14-26

/11/ Casassa, E.F. : Separation Science, 6(2), **1971**, 305-319

/12/ Casassa, E.F. : Polymer Letters, 5, **1967**, 773-778

/13/ Halasz, I. ; Vogtel, P. : Angewandte Chemie 92, **1980**,25-29

/14/ Halasz, I. ; Kornel, M. : Angewandte Chemie Int. Ed. Engl 17, **1978**,901-908

/15/ Haller, W. : Macromolecules, 10(1), **1977**, 83-86

/16/ Haller, W. : Nature, 206, **1965**, 693-696

/17/ Carslaw, H.S. ; Jaeger, J.C. : Conduction of Heat in Solids
Oxford at teh Clarendon Press, **1959**, Second Edition

/18/ Yau, W.W., Ginnard, C.R., Kirkland, J.T. : Journal of
Chromatography, 149, **1978**, 465-487

/19/ Gorbunov, A.A. ; Solovyova, L.Ya. ; Pasechnik, V.A. :
Vysokomolekyarnye Soedineniya, Seriya A, 26, **1984**, 967

/20/ Balke, S.T. : Journal of Chromatography Library-Volume 29
1984, edited by Balke, S.T., Chapter 5, 193-240

/21/ Hamilton, R.J. ; Sewell, P.A. : Introduction to High Performance Liquid Chromatography,**1982** Chapman and Hall, London New York

/22/ Provencher, S.W. : Makromolekulare Chemie, **1979**, 180, 201-209

/23/ Provencher, S.W. : Computer Physics Communications, **1982**, 27, 213-227

/23/ Provencher, S.W. : Computer Physics Communications, **1982**, 27, 229-242

/25/ Provencher, S.W. : Technical Report EMBL-DA07 (March 1984) CONTIN (Version 2) User's Manual

10. Figures

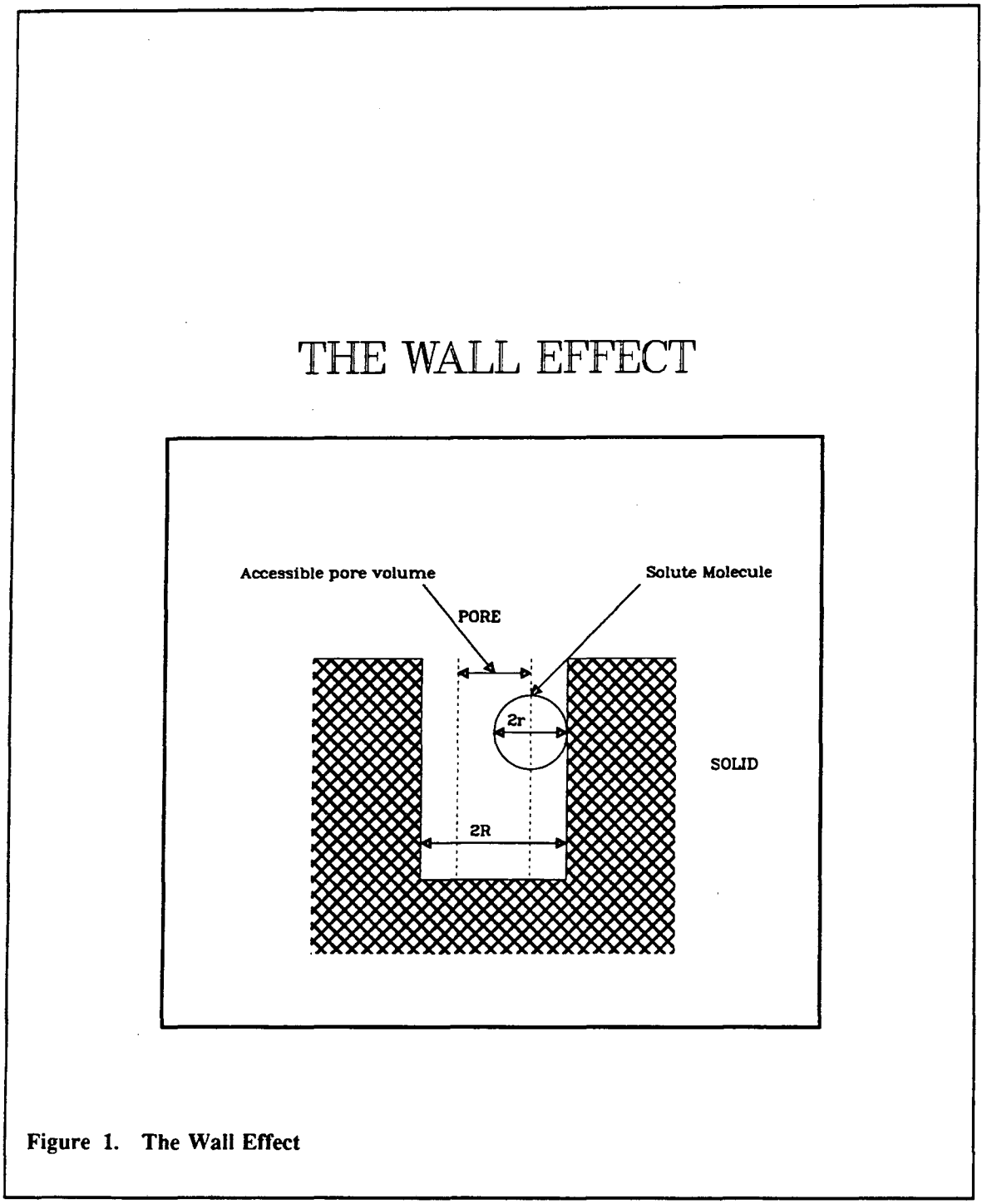

Figure 1. The Wall Effect

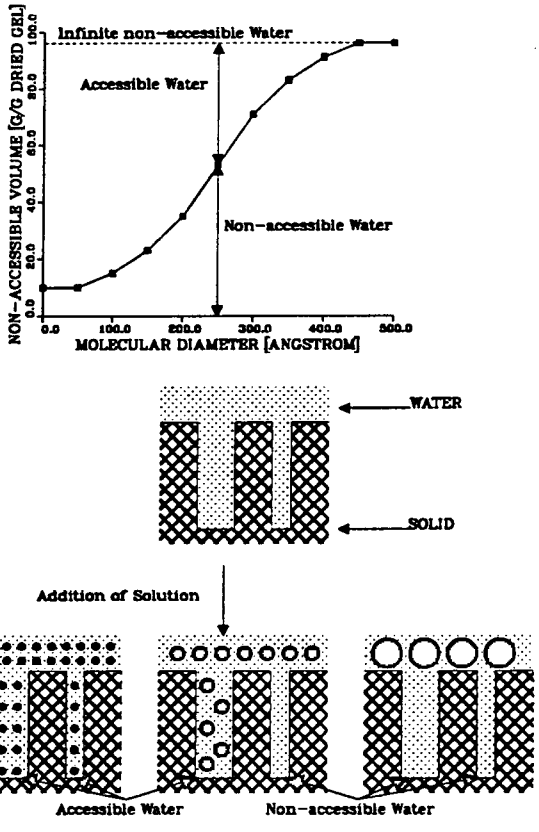

Figure 2. The cumulative non-accessible imbibed liquid as a function of molecular radius.

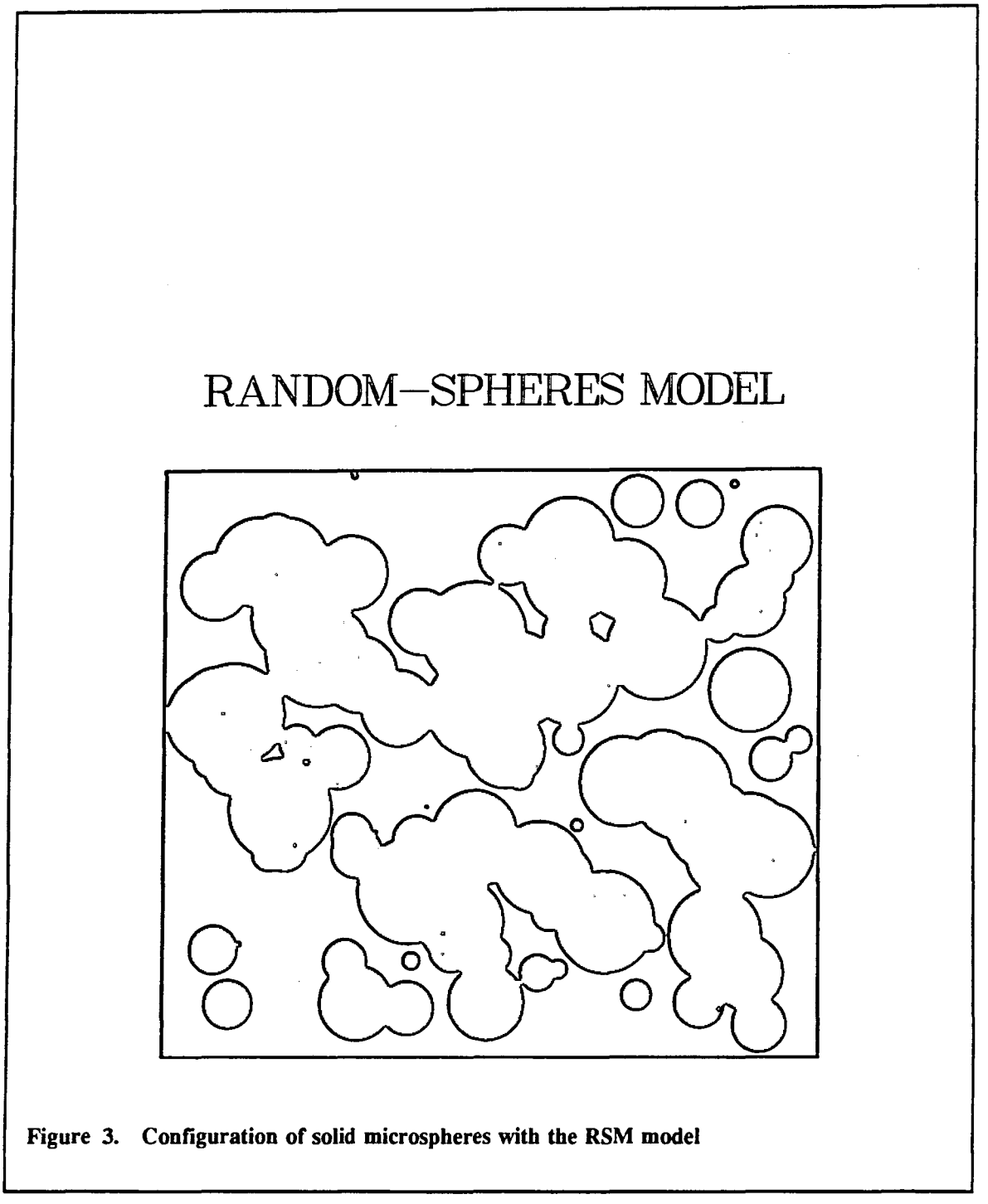

Figure 3. Configuration of solid microspheres with the RSM model

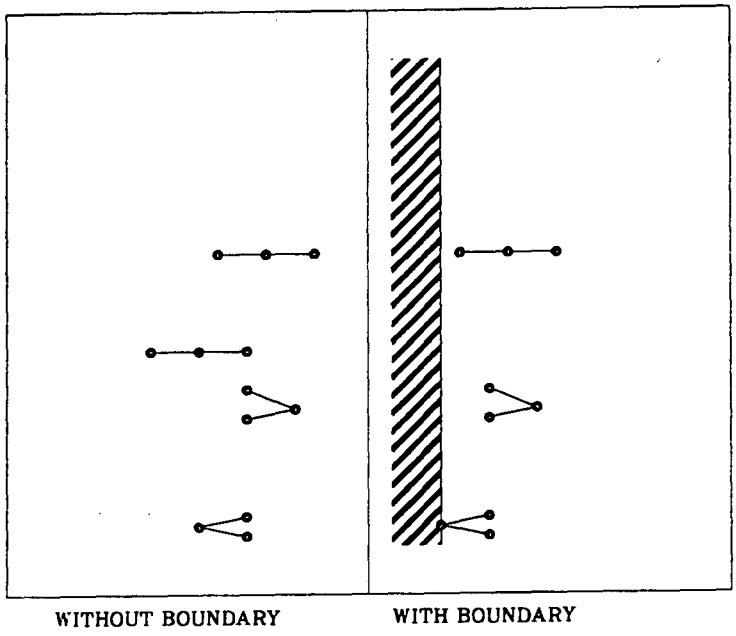

Figure 4. Number of conformations for a two-step polymer

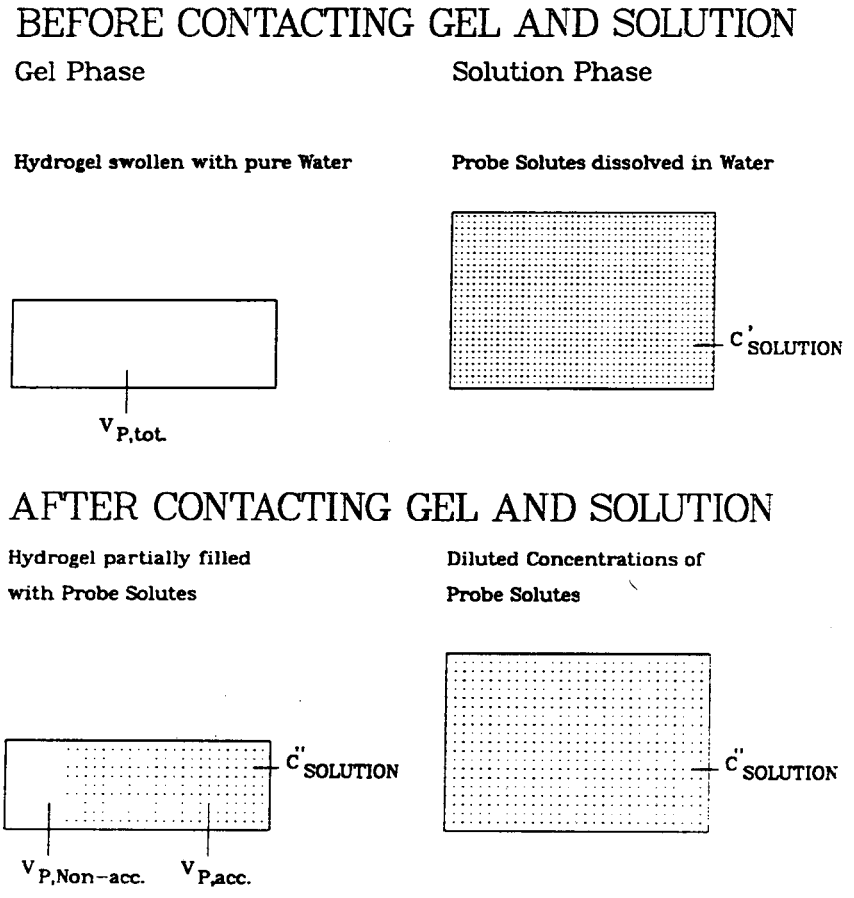

Figure 5. General definition of the distribution coefficient

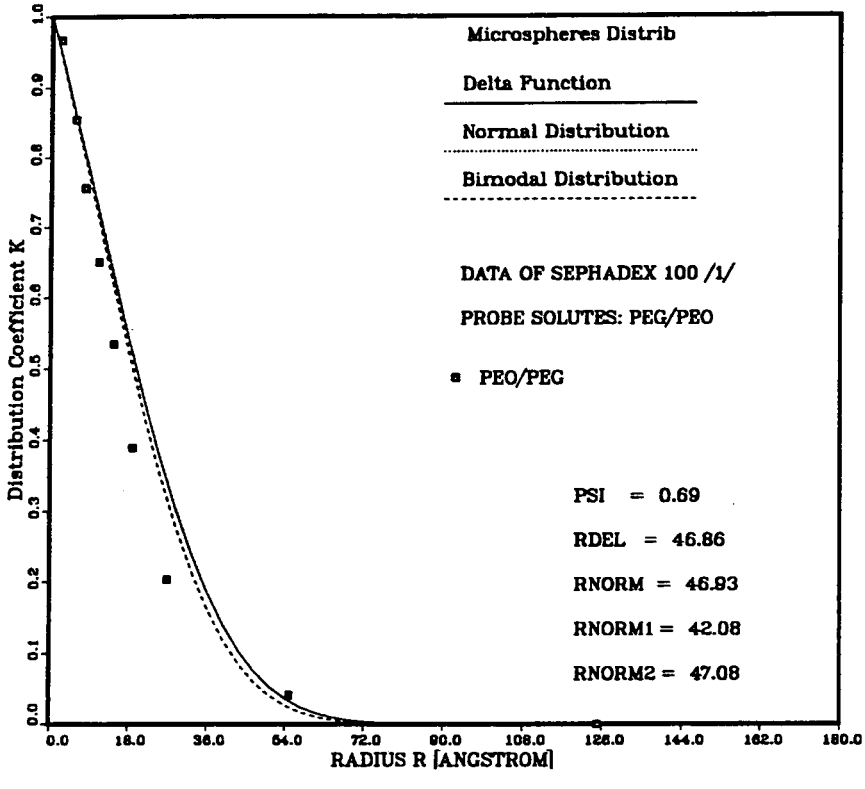

Figure 6. Distribution coefficient for Sephadex G-100, PEG/PEO series

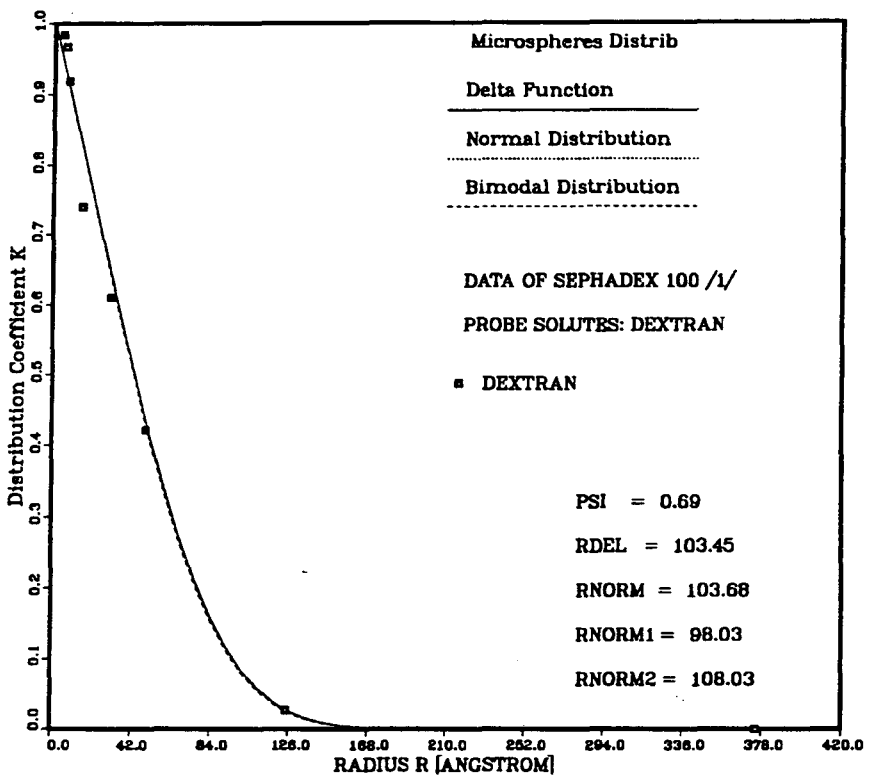

Figure 7. Distribution coefficient for Sephadex G-100, Dextran series

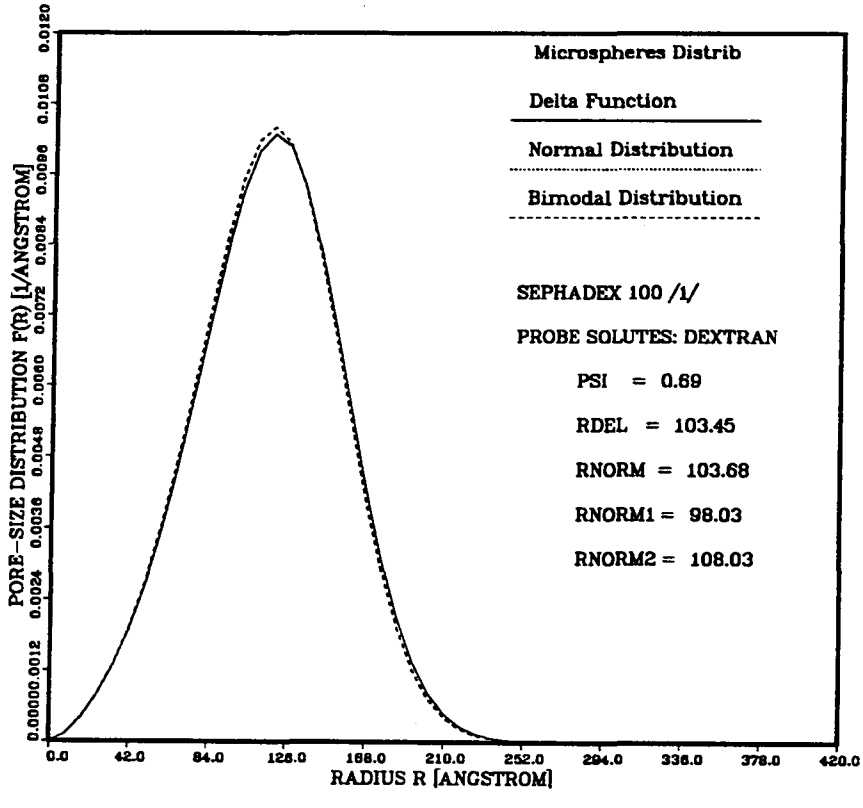

Figure 8. Pore-size distribution for Sephadex G-100, Dextran series

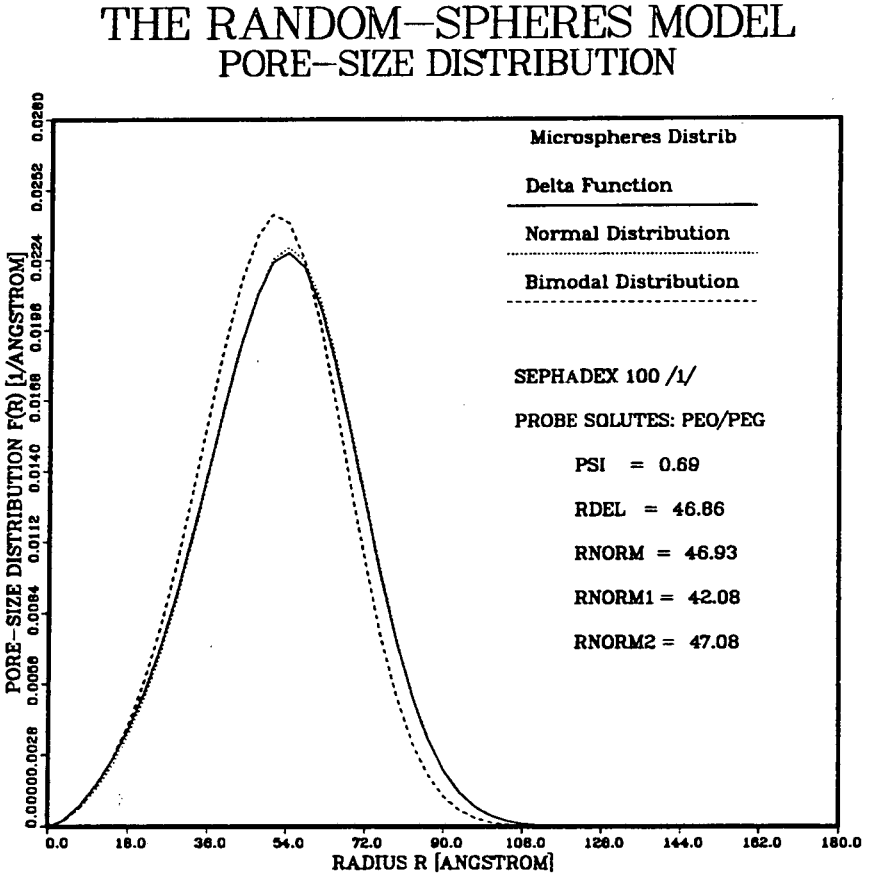

Figure 9. Pore-size distribution for Sephadex G-100, PEO/PEG series

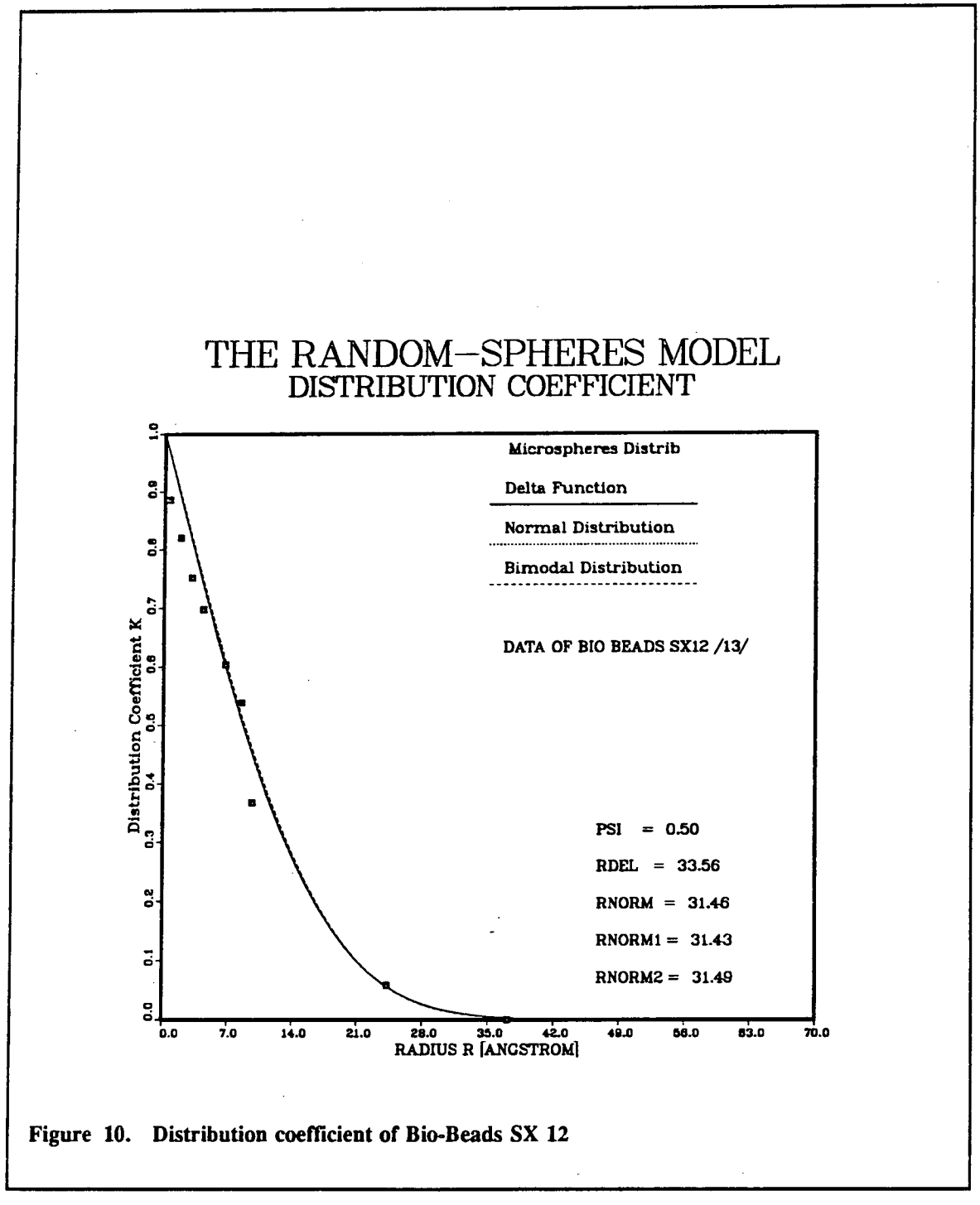

Figure 10. Distribution coefficient of Bio-Beads SX 12

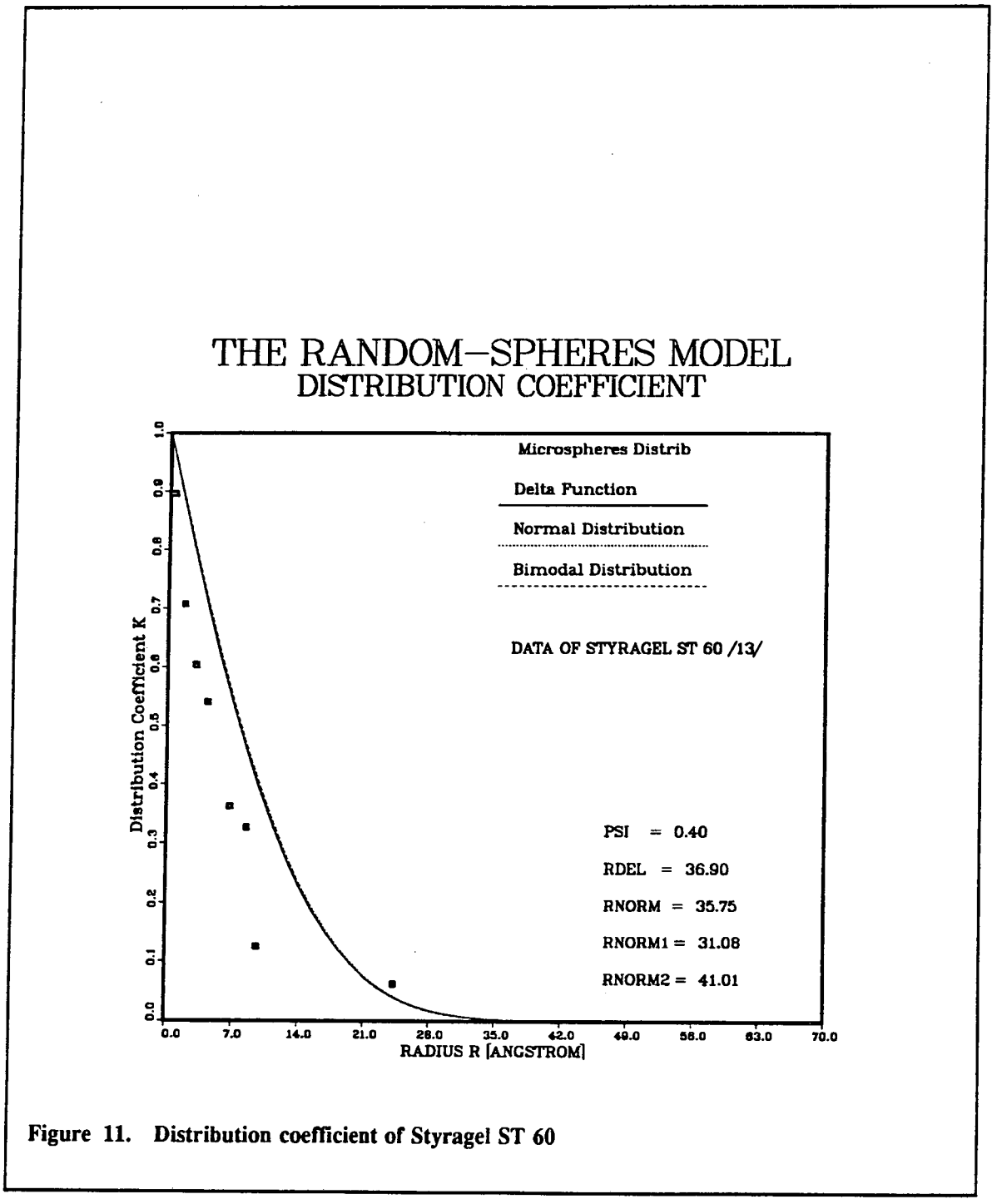

Figure 11. Distribution coefficient of Styragel ST 60

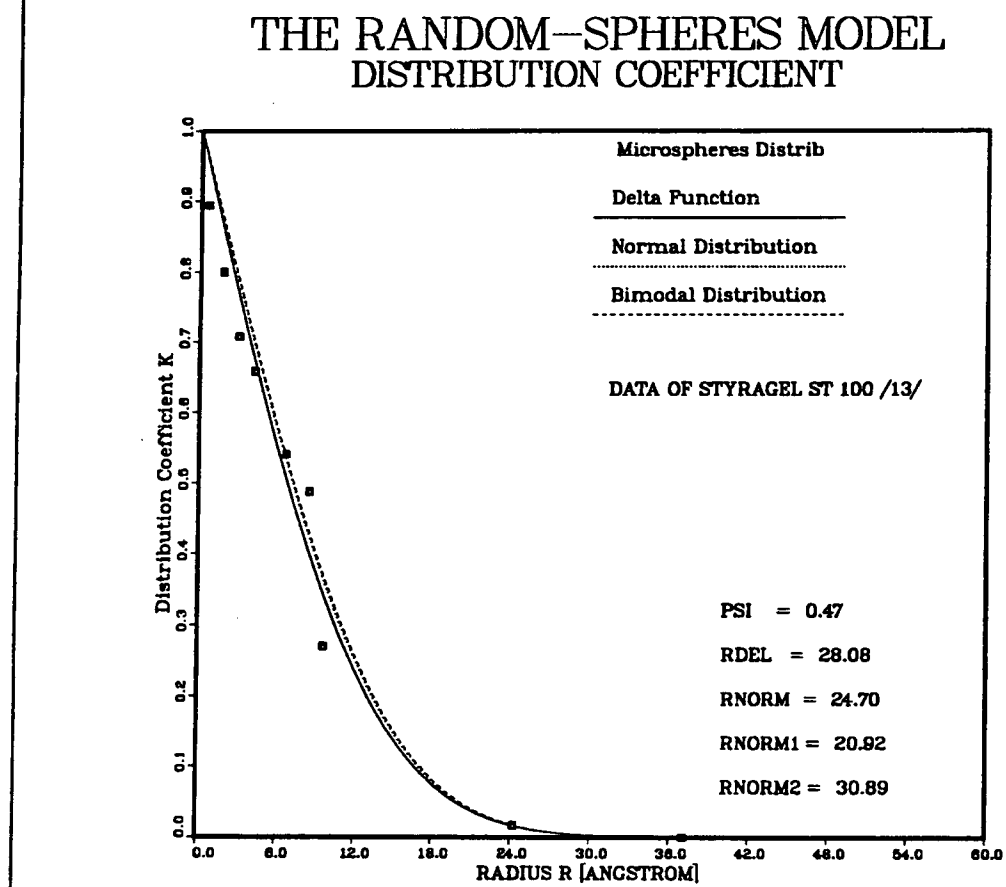

Figure 12. Distribution coefficient of Styragel ST 100

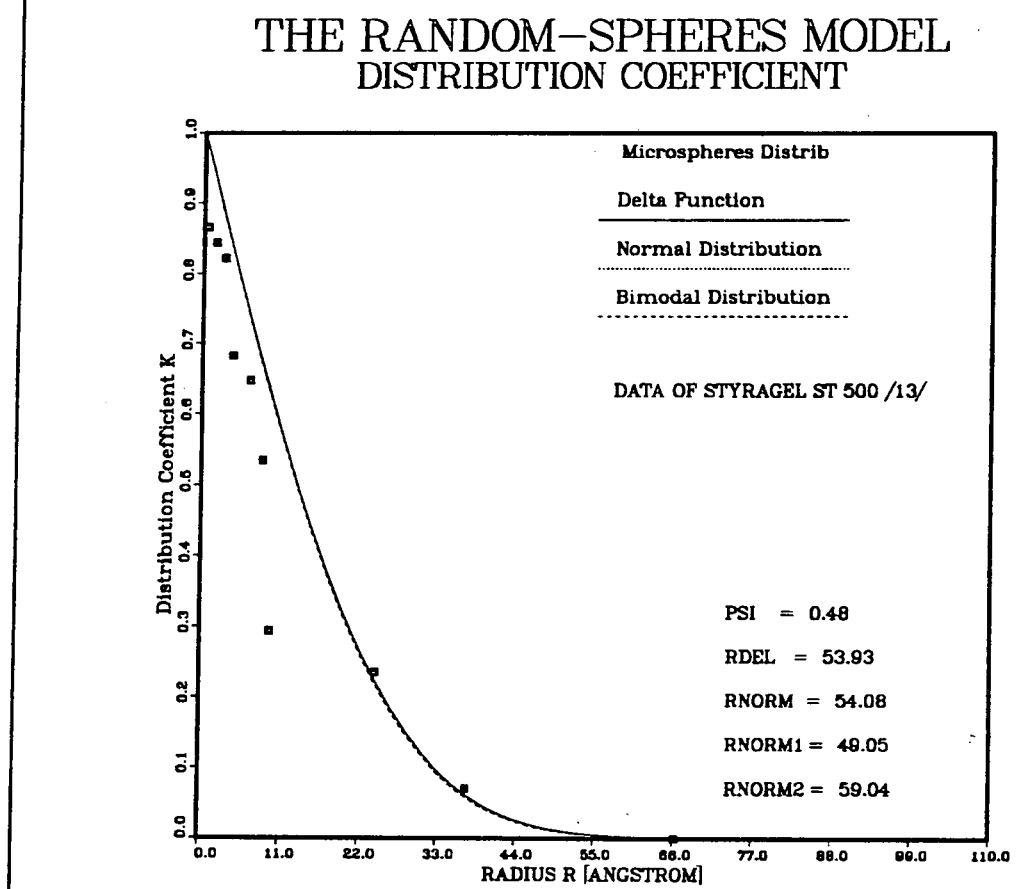

Figure 13. Distribution coefficient of Styragel ST 500

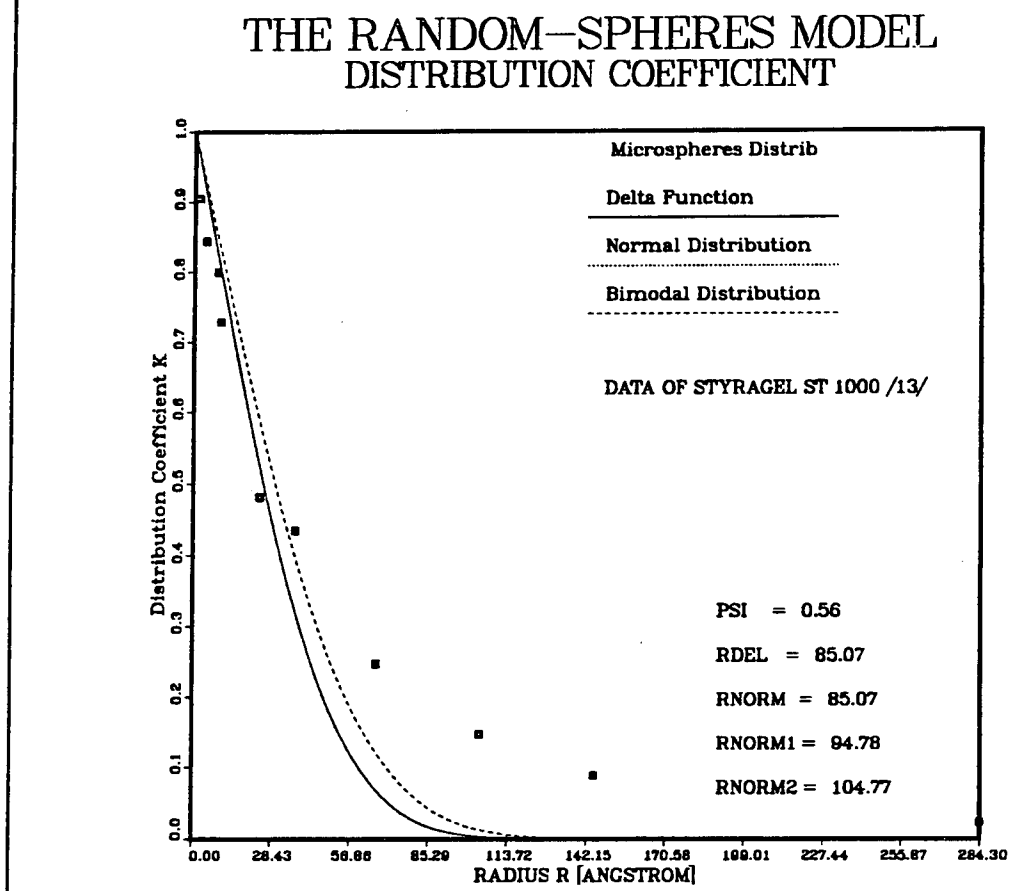

Figure 14. Distribution coefficient of Styragel ST 1000

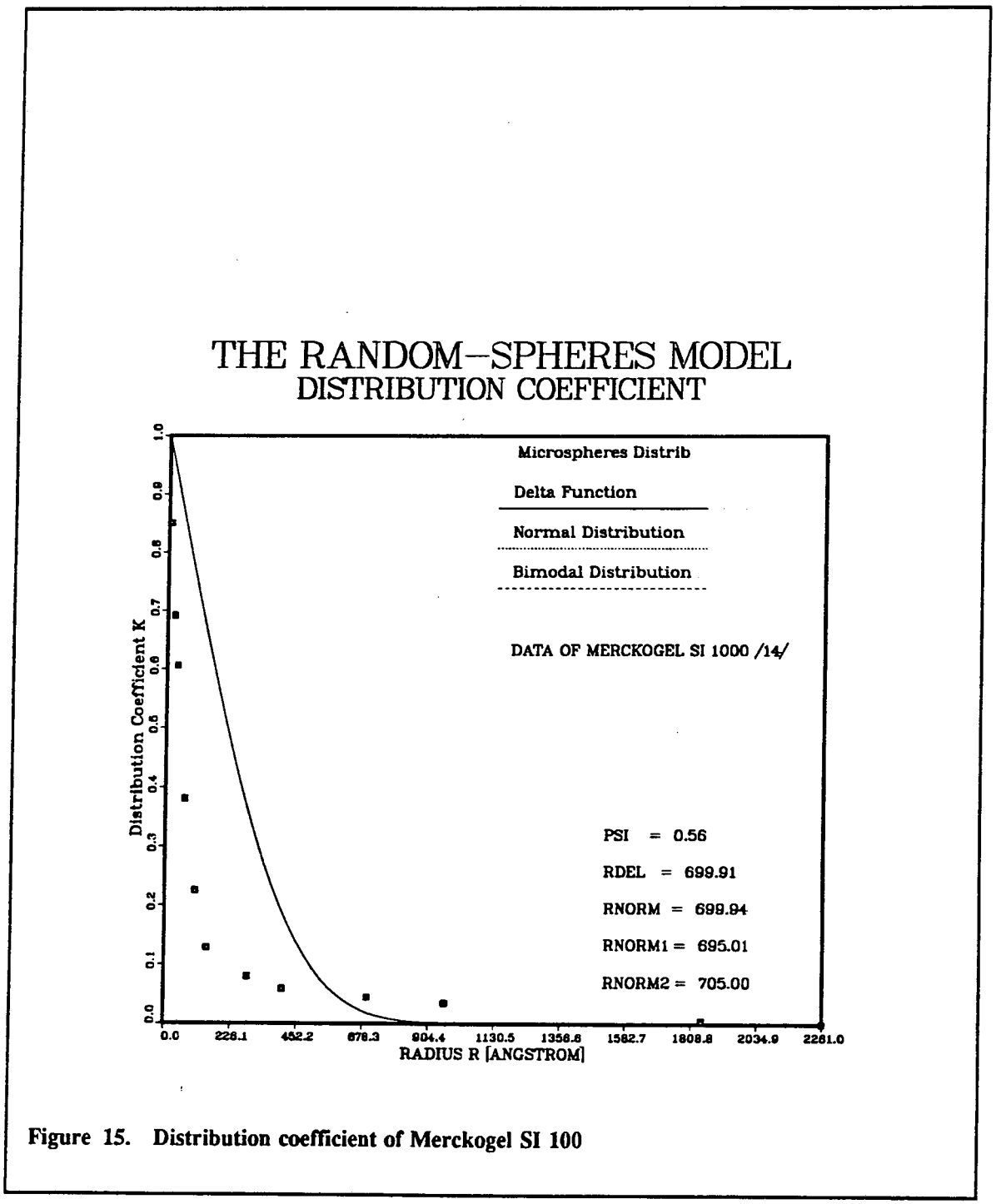

Figure 15. Distribution coefficient of Merckogel SI 100

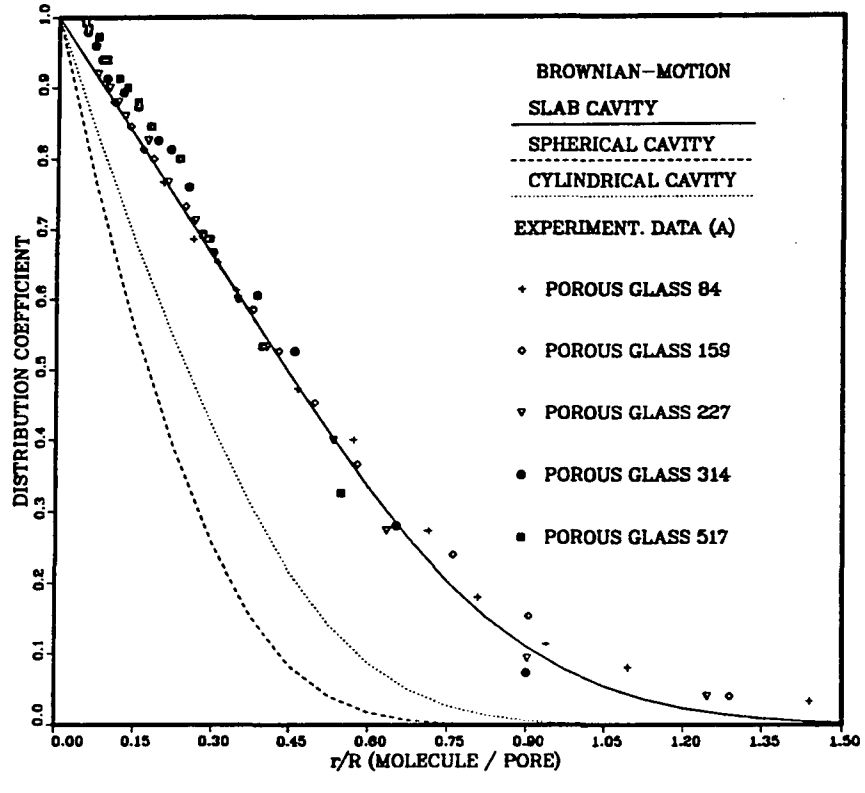

Figure 16. Theoretical-distribution function K(r,R) for three geometric cavities

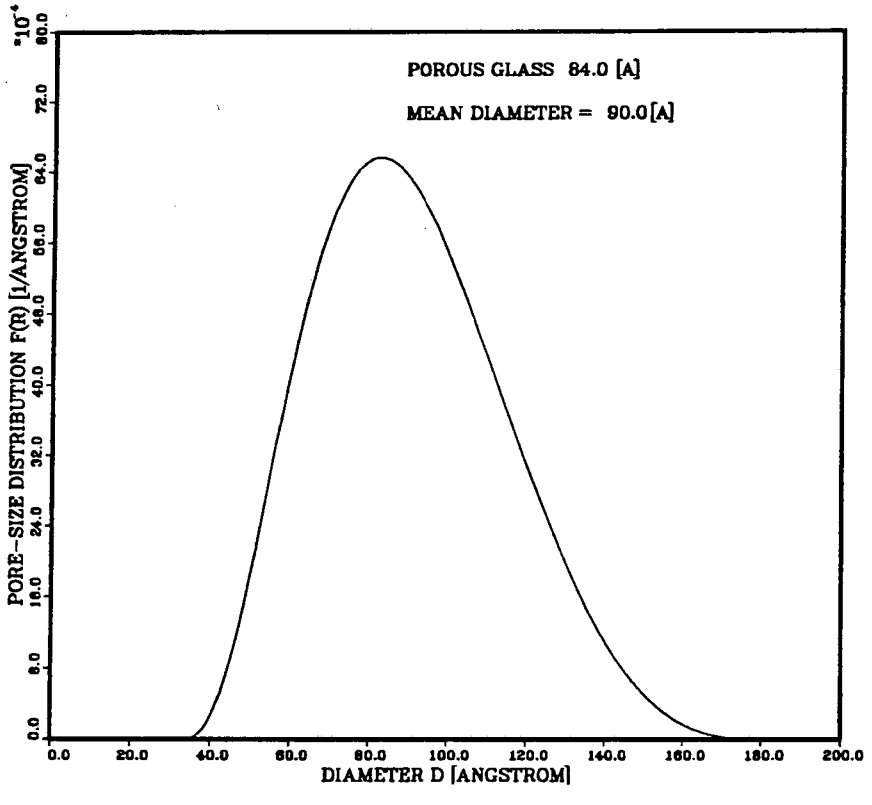

Figure 17. Pore-size distribution of Porous Glass 84

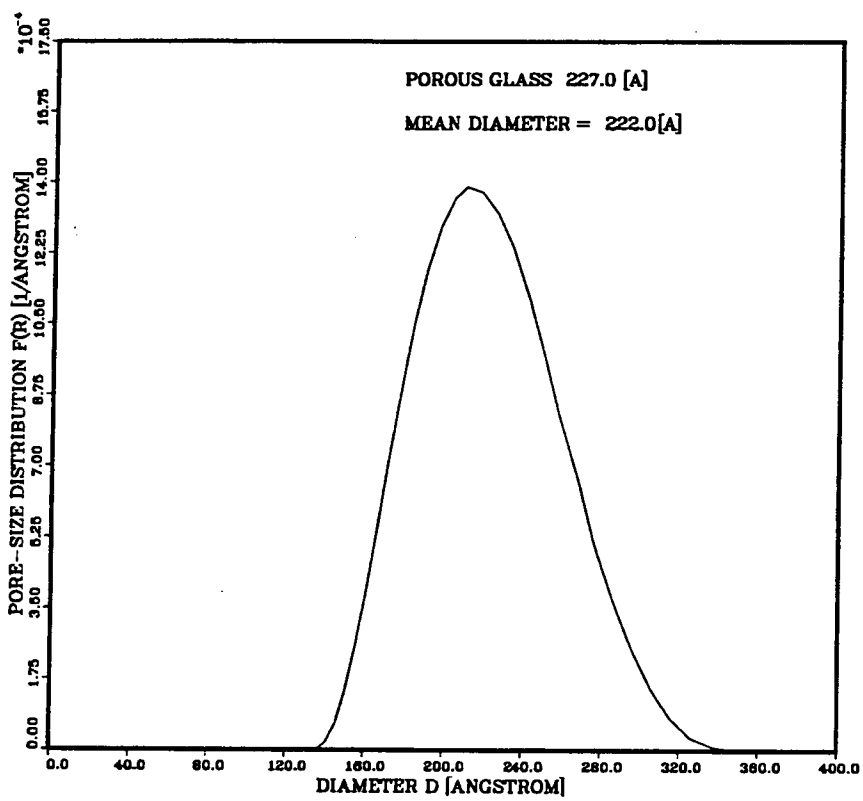

Figure 18. Pore-size distribution of Porous Glass 227

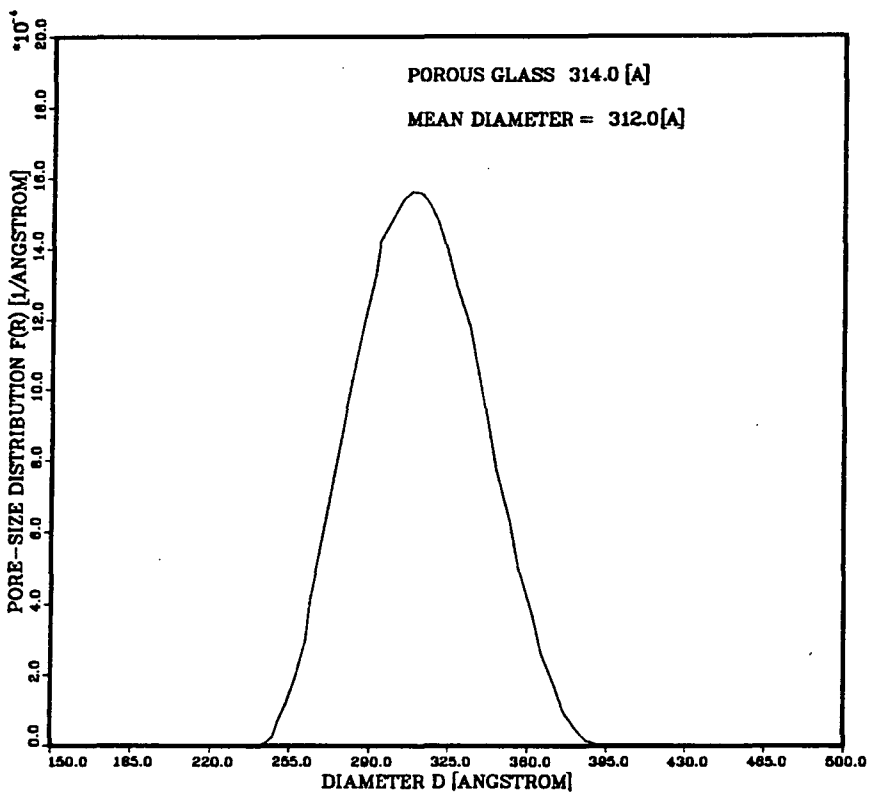

Figure 19. Pore-size distribution of Porous Glass 314

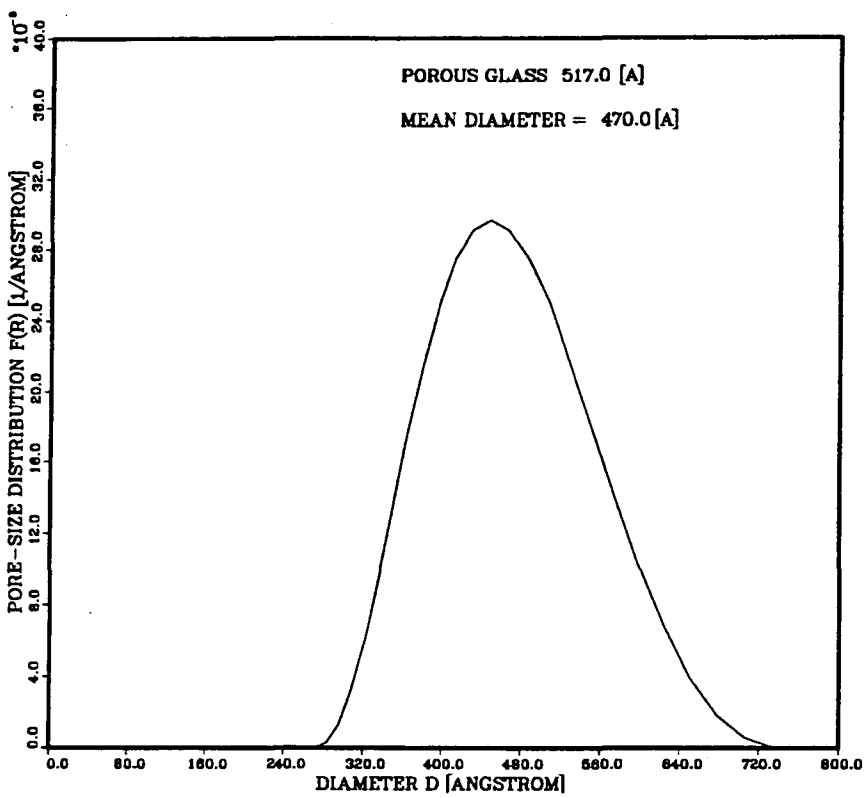

Figure 20. Pore-size distribution of Porous Glass 517

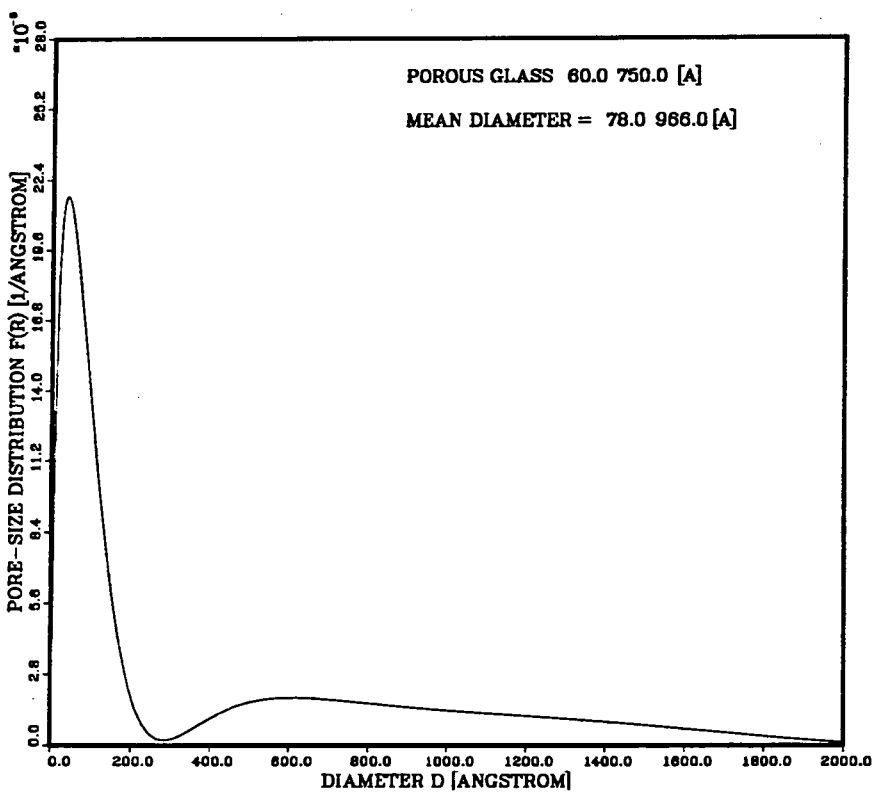

Figure 21. Pore-size distribution of Porous Glass Mixture 60, 750

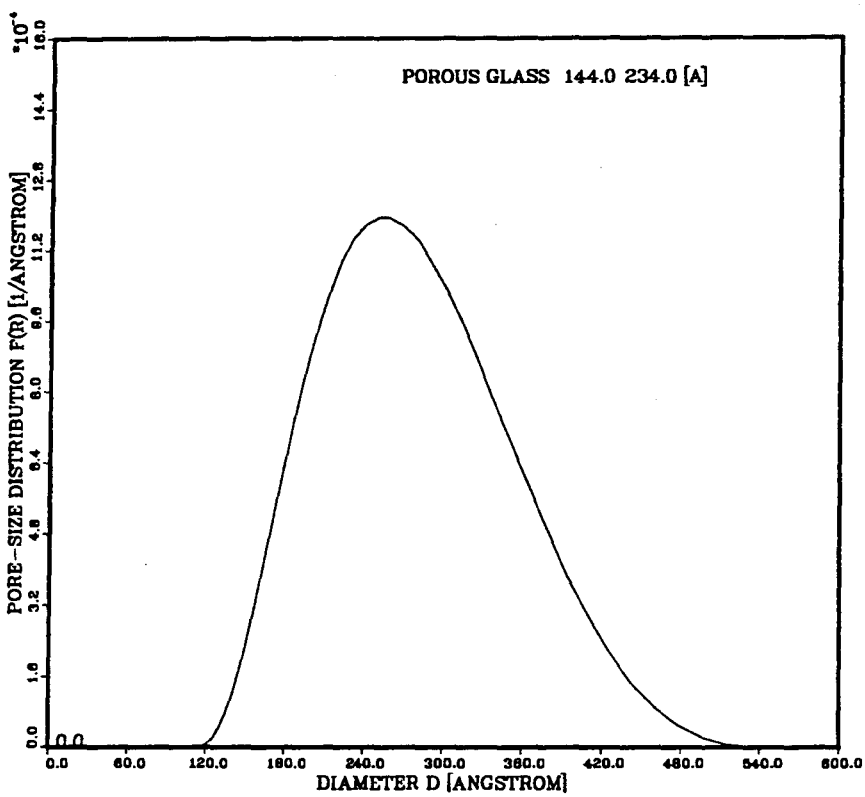

Figure 22. Pore-size distribution of Porous Glass Mixture 144, 234

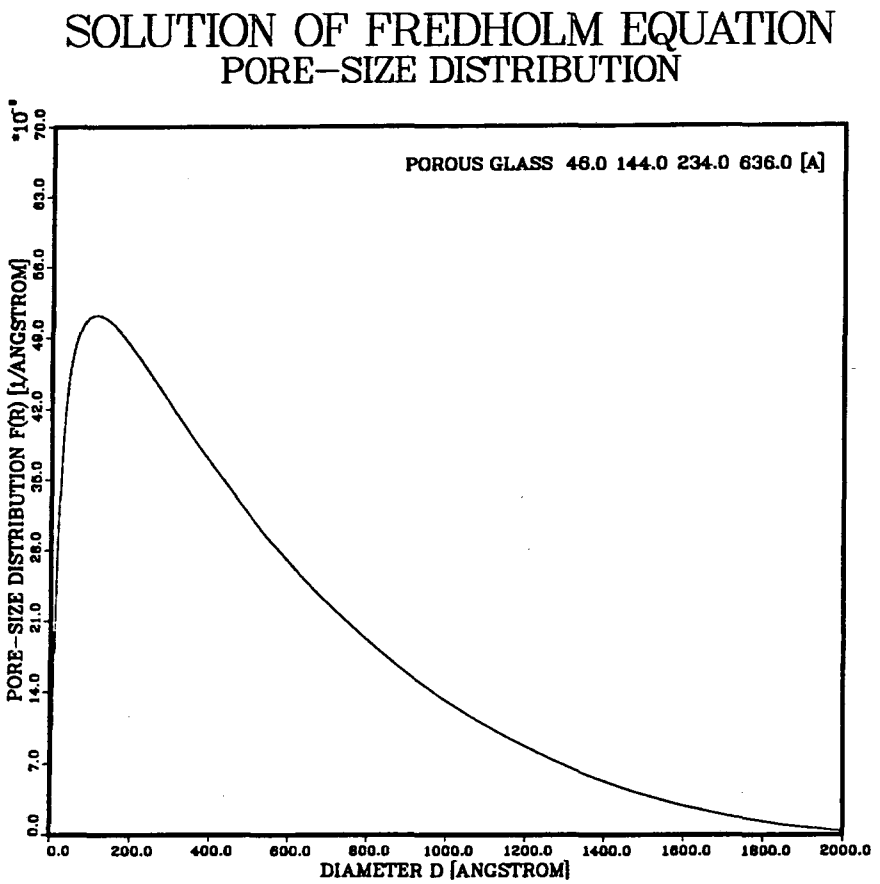

Figure 23. Pore-size distribution of Porous Glass Mixture 46, 144, 234, 626

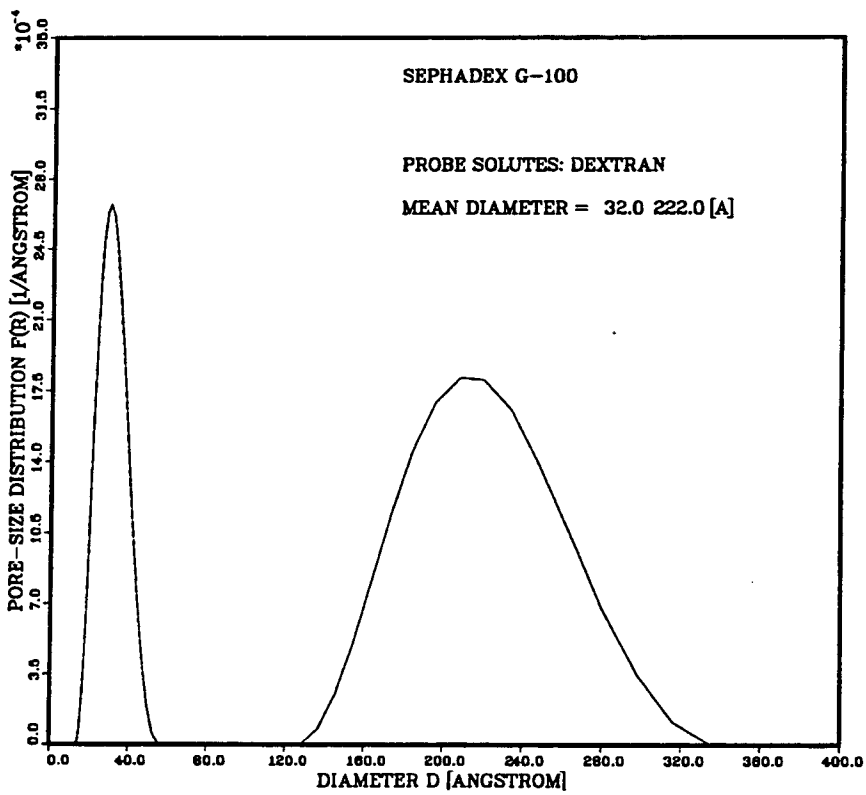

Figure 24. Pore-size distribution of Sephadex , Dextran series

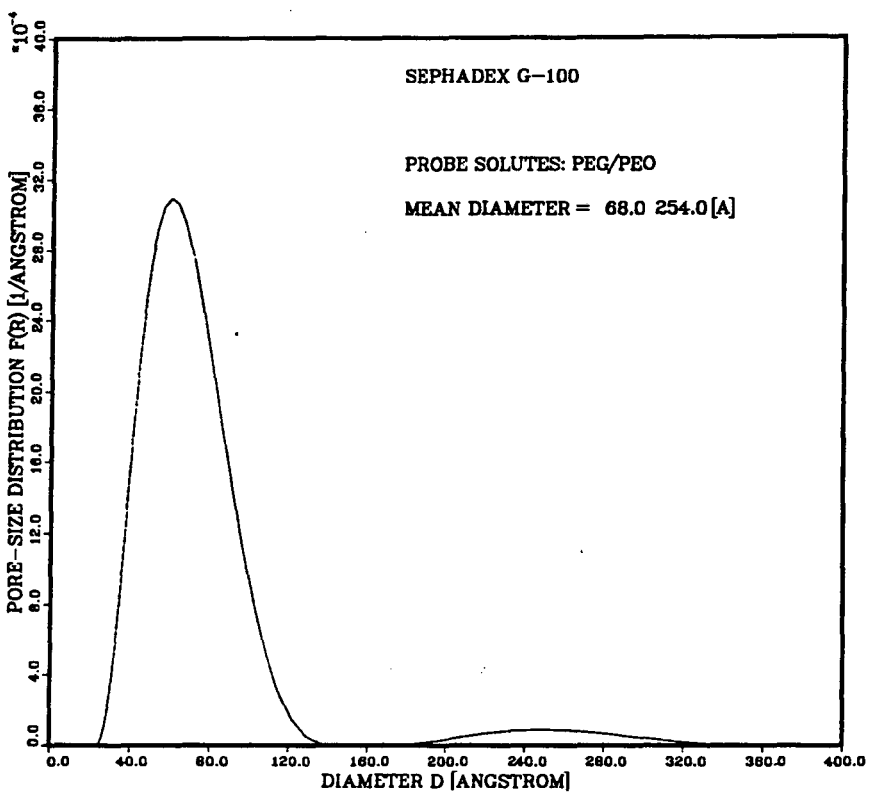

Figure 25. Pore-size distribution of Sephadex , PEO/PEG series

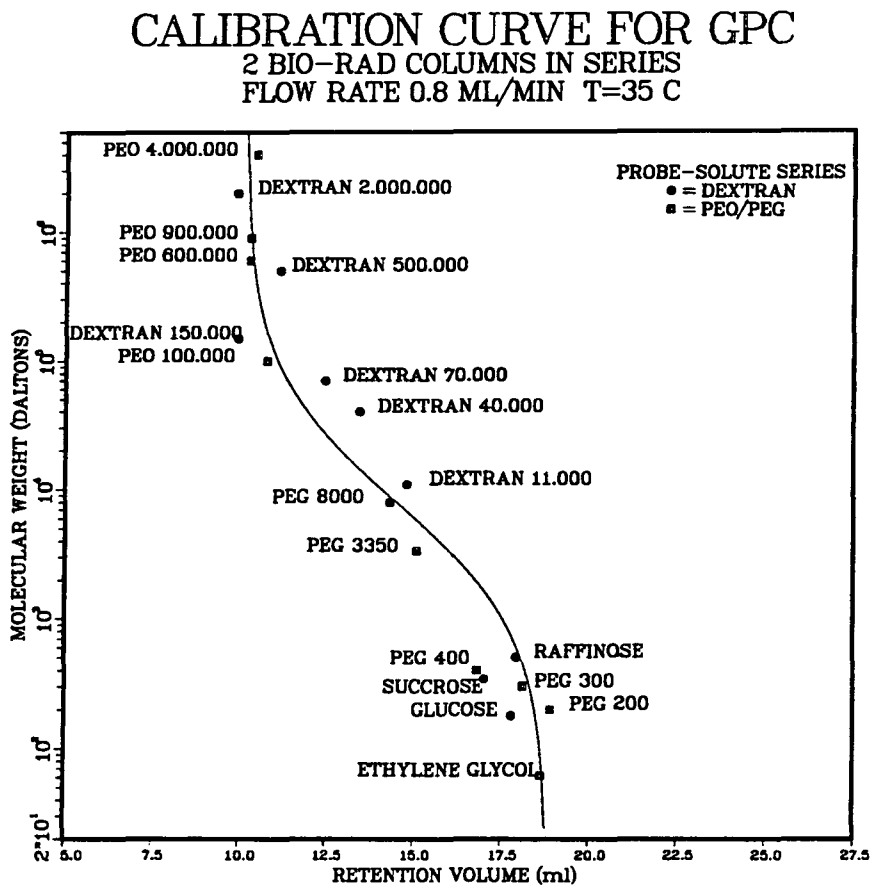

Figure 26. Calibration Graph for the PEO/PEG and Dextran solutes

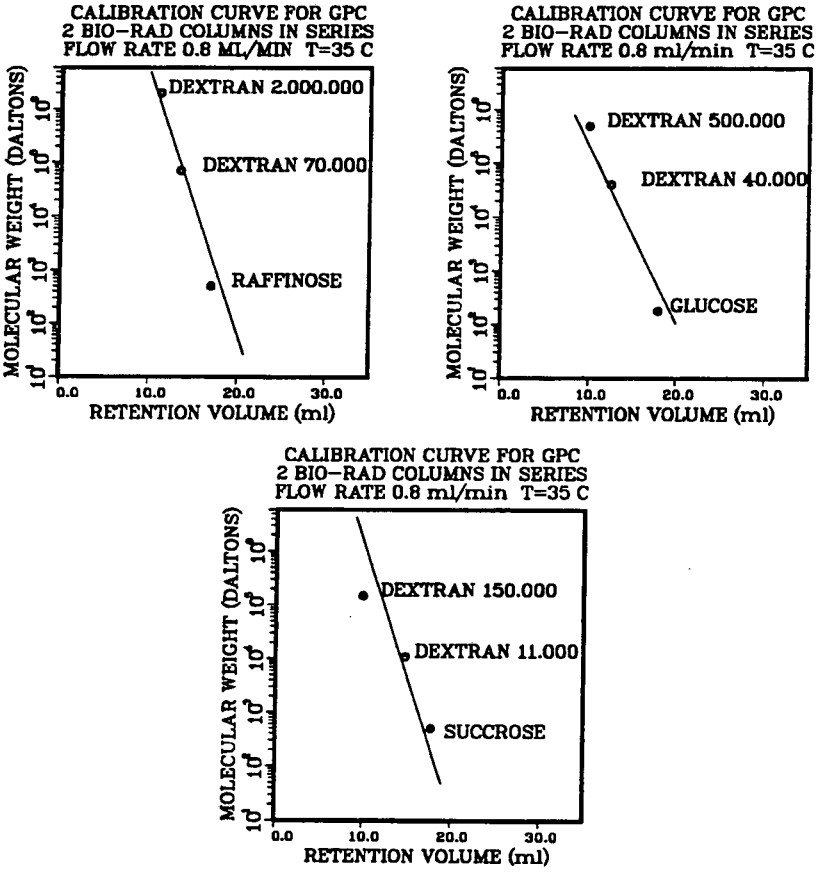

Figure 27. Single Calibration Graphs for the Dextran series

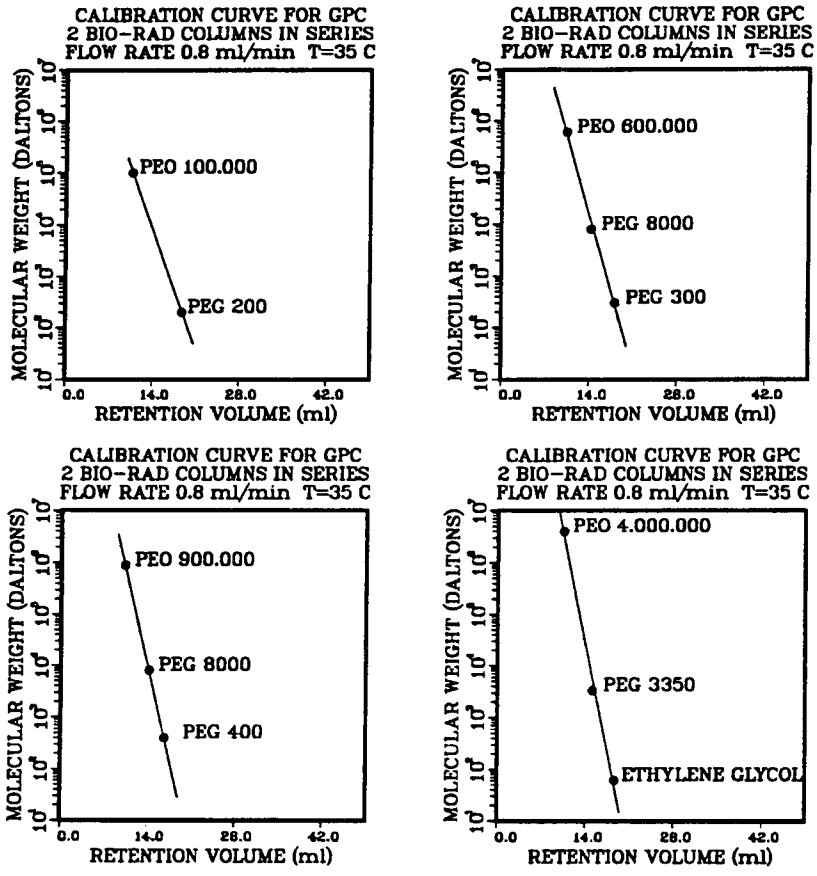

Figure 28. Single Calibration Graphs for the PEO/PEG series

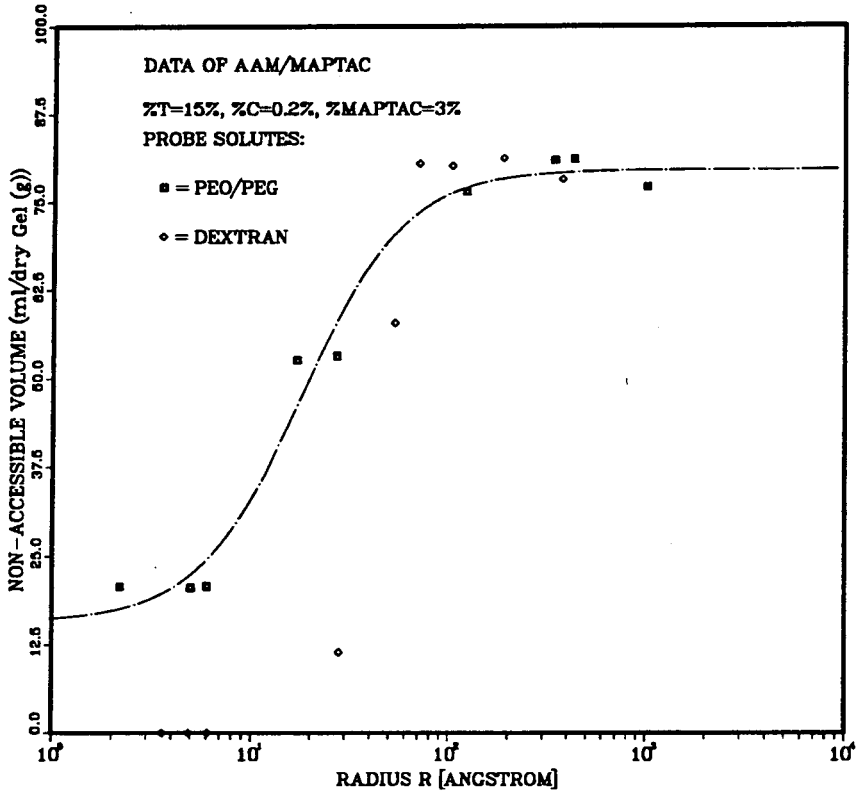

Figure 29. Cumulative pore volume for AAm/MAPTAC Hydrogel, PEO/PEG- and Dextran series

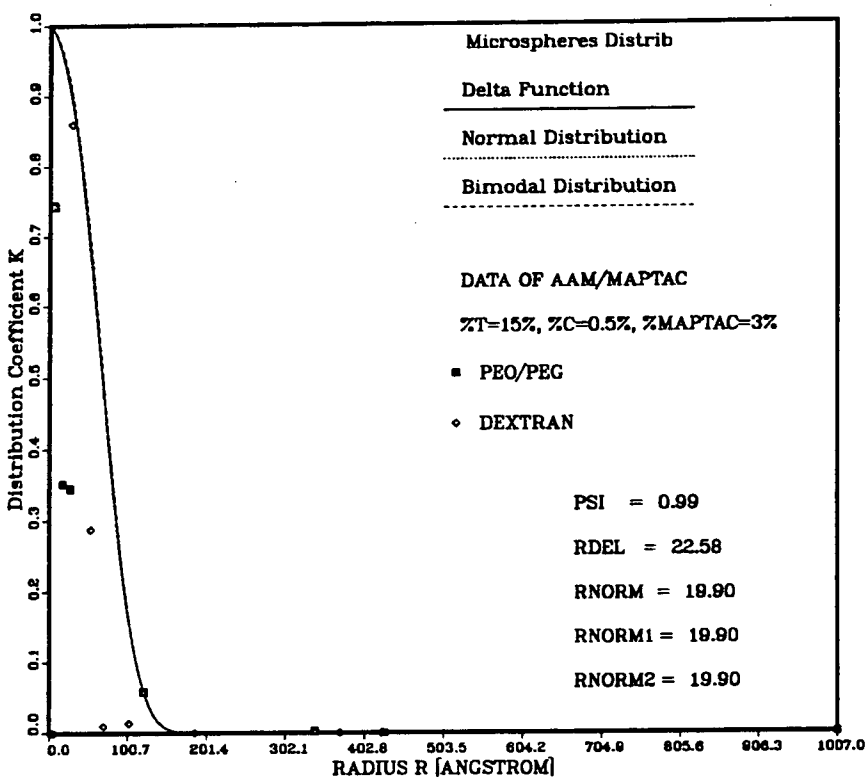

Figure 30. Distribution-coefficient of AAm/MAPTAC Hydrogel, PEO/PEG- and Dextran series

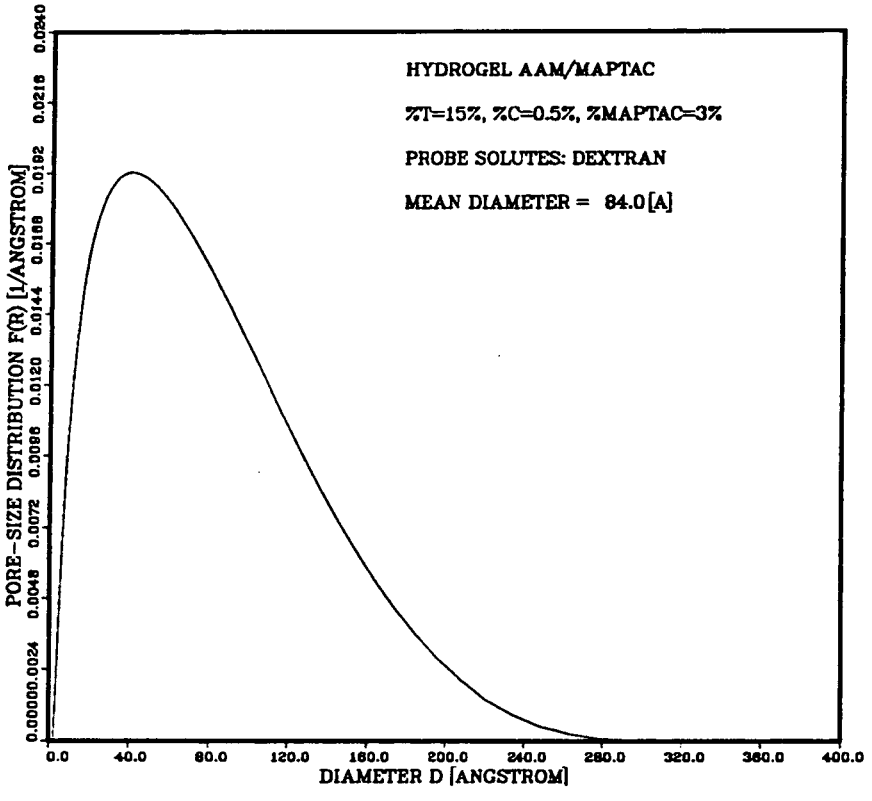

Figure 31. Pore-size distribution for AAm/MAPTAC Hydrogel, Dextran series

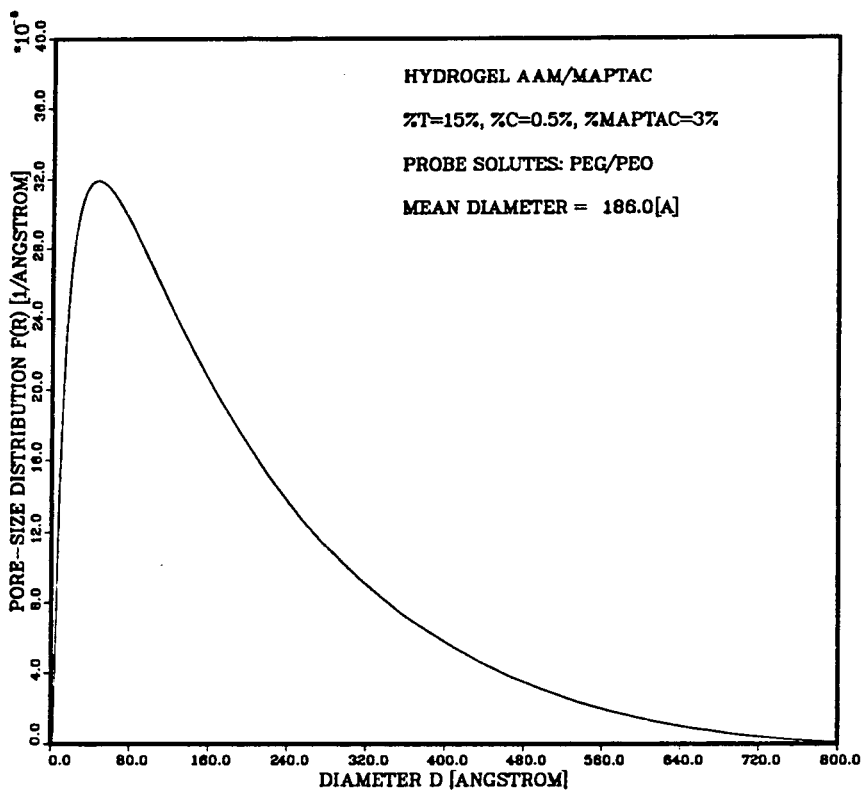

Figure 32. Pore-size distribution for AAm/MAPTAC Hydrogel, PEO/PEG series

LAWRENCE BERKELEY LABORATORY
UNIVERSITY OF CALIFORNIA
TECHNICAL INFORMATION DEPARTMENT
BERKELEY, CALIFORNIA 94720